The class XIV myosin of *Toxoplasma gondii*, TgMyoA, is druggable in an animal model of infection

Anne Kelsen*[1], Robyn S Kent*[1], Anne K Snyder[1], Eddie Wehri[2], Stephen J Bishop[3], Rachel V Stadler[1], Cameron Powell[4], Bruno Martorelli di Genova[1], Pramod K Rompikuntal[1], Martin J Boulanger[4], David M Warshaw[5], Nicholas J Westwood[3], Julia Schaletzky[2], Gary E Ward[1†]

[1] Department of Microbiology and Molecular Genetics, University of Vermont Larner College of Medicine, Burlington, Vermont, USA

[2] Center for Emerging and Neglected Diseases, University of California Berkeley, California, USA

[3] School of Chemistry and Biomedical Sciences Research Complex, University of St. Andrews and EaStCHEM, St Andrews, Fife, Scotland, United Kingdom

[4] Department of Biochemistry and Microbiology, University of Victoria, Victoria, BC, Canada

[5] Department of Molecular Physiology and Biophysics, University of Vermont Larner College of Medicine, Burlington, Vermont, USA

* These authors contributed equally to the work

† Communicating author: Gary.Ward@uvm.edu

Abstract

Toxoplasma gondii is a widespread apicomplexan parasite that can cause severe disease in its human hosts. The ability of *T. gondii* and other apicomplexan parasites to invade into, egress from, and move between cells of the hosts they infect is critical to parasite virulence and disease progression. An unusual and highly conserved parasite myosin motor (TgMyoA) plays a central role in *T. gondii* motility. The goal of this work was to test whether pharmacological inhibition of TgMyoA can alter disease progression in an animal model of infection. To this end, we sought to identify small molecule inhibitors of TgMyoA by screening a collection of 50,000 structurally diverse small molecules for inhibitors of the recombinant motors actin-activated ATPase activity. The top hit to emerge from the screen, KNX-002, inhibited TgMyoA with little to no effect on any of the vertebrate myosins tested. KNX-002 was also active against parasites, inhibiting parasite motility and growth in culture in a dose-dependent manner. We used chemical mutagenesis, selection in KNX-002, and targeted sequencing to identify a mutation in TgMyoA (T130A) that renders the recombinant motor less sensitive to compound. Compared to wild-type parasites, parasites expressing the T130A mutation showed reduced sensitivity to KNX-002 in motility and growth assays, confirming TgMyoA as a biologically relevant target of KNX-002. Finally, KNX-002 was shown to slow disease progression in mice infected with wild-type parasites, but not parasites expressing the resistance-conferring TgMyoA T130A mutation. These data demonstrate the specificity of KNX-002 for TgMyoA, both *in vitro* and *in vivo*, and validate TgMyoA as a druggable target for toxoplasmosis. Since TgMyoA is essential for virulence, conserved in apicomplexan parasites, and distinctly different from the myosins found in humans, pharmacological inhibition of MyoA offers a promising new approach to treating the devastating diseases caused by *T. gondii* and other apicomplexan parasites.

Introduction

Nearly one third of the world's population are or have been infected with the apicomplexan parasite, *Toxoplasma gondii*. Although most infections are subclinical, acute toxoplasmosis can have severe consequences in neonates and immunocompromised individuals. Congenital infection can lead to spontaneous abortion or stillbirth, and even children born with subclinical infection frequently experience sequelae later in life including neurological damage and vision impairment [1, 2]. Among the immunocompromised, toxoplasmic encephalitis is a particularly significant risk in AIDS patients who are unaware of their HIV status [3-5] and in the ~50% of HIV-infected individuals worldwide who do not have access to antiretroviral therapy [6, 7]. In individuals with AIDS, adverse effects of the currently available drugs to suppress toxoplasmosis [8] cause the discontinuation of treatment in up to 40% of patients [4, 9-11], highlighting the need for new, better-tolerated drugs to reduce toxoplasmosis-related morbidity and mortality.

Within the brain and other tissues of a patient suffering from active toxoplasmosis, the tachyzoite stage of the parasite uses a unique form of substrate-dependent "gliding" motility to invade into and egress from the cells of its host, to spread throughout the patient's tissues, and to migrate across

biological barriers [12-15]. *T. gondii* tachyzoites move in the extracellular matrix along flattened corkscrew-like trajectories, with regularly repeating periods of acceleration and deceleration [16]. The mechanisms underlying gliding motility are thought to be conserved among apicomplexan parasites, including *Plasmodium spp.* (the causative agents of malaria) and *Cryptosporidium spp.* (which cause severe diarrheal disease). Motility is driven, at least in part, by an unusual class XIVa myosin motor protein, myosinA (MyoA), found only in apicomplexan parasites and a few ciliates. In *T. gondii,* this motor consists of the TgMyoA heavy chain and two associated light chains, TgMLC1 and either TgELC1 or TgELC2 [17-19]. TgMyoA is a single-headed motor with a very low duty ratio (*i.e.*, it remains strongly bound to actin for only ~1% of its catalytic cycle) yet moves actin filaments at the same speed as skeletal muscle myosin, a double-headed motor with a 5-fold higher duty ratio [20, 21]. TgMyoA lacks a conventional tail, as well as several residues conserved in other myosins that normally function to regulate actomyosin activity [22, 23], and employs atypical strategies for chemomechanical coupling and force transduction [24, 25].

Depletion of *TgMyoA* results in severely reduced parasite motility, host cell invasion, and host cell egress [26-29]. As a result, parasites lacking TgMyoA are avirulent in an animal model of infection [28]. Despite its importance in the *T. gondii* life cycle, we know little about how TgMyoA generates the complex pattern of parasite motility seen in 3D or how TgMyoA function contributes to disease pathogenesis in an infected host. Because the parasite can compensate for the loss or reduced expression of proteins important to its life cycle [30-32], small-molecule inhibitors of TgMyoA would serve as valuable complementary tools for determining how different aspects of motor function contribute to parasite motility and the role played by TgMyoA in parasite dissemination and virulence. Specific inhibitors are also necessary to establish TgMyoA as a “druggable” target, *i.e.*, a protein whose activity is amenable to inhibition by small molecules, and to test whether pharmacological inhibition of TgMyoA activity *in vivo* alters the course of an infection.

We describe here the identification and characterization of KNX-002, the first specific inhibitor of an apicomplexan Class XIVa myosin. KNX-002 inhibits TgMyoA motor activity, parasite motility, and parasite growth in culture in a dose-dependent manner, with little or no effect on a variety of other vertebrate myosins. On-target activity in parasites was confirmed by identifying a mutation in TgMyoA that rescues parasite motility and growth in the presence of the compound. The availability of a specific inhibitor of TgMyoA, together with isogenic parasite strains that show differential sensitivity to the compound, enabled us to undertake the first direct test of whether pharmacological inhibition of MyoA can be used to alter the progression of disease caused by an apicomplexan parasite.

Results

High-throughput screening identifies a novel inhibitor of TgMyoA. To identify inhibitors of TgMyoA motor activity, we used our previously described method for producing large amounts of functional motor, in which the TgMyoA heavy chain is co-expressed in insect cells with its two light chains, TgMLC1 and TgELC1, and a myosin co-chaperone protein [33]. We developed a miniaturized

117 coupled enzyme assay to measure actin-dependent ATPase activity of the purified recombinant motor
118 and screened 50,000 compounds from the compound library at Cytokinetics, Inc., for inhibitors of this
119 ATPase activity. Hit follow-up and characterization included dose-response analysis using resupplied
120 compound that was determined to be >95% pure by LC/MS analysis and control assays demonstrating
121 the compound was inactive against an unrelated ATPase, hexokinase. The most potent hit was 1-(4-
122 methoxyphenyl)-N-((3-(thiophen-2-yl)-1H-pyrazol-4-yl)methyl)cyclopropan-1-amine (Figure 1A, inset),
123 subsequently named KNX-002. KNX-002 inhibits TgMyoA ATPase activity in a dose-dependent manner
124 with an IC_{50} of 2.8 μM (95% C.I. 2.4-3.2 μM; Figure 1A). In contrast, KNX-002 has little to no detectable
125 effect on the actin-activated ATPase activity of bovine cardiac myosin, chicken gizzard smooth muscle
126 myosin, rabbit fast skeletal muscle myosin, or bovine slow skeletal muscle myosin, up to the highest
127 concentrations tested (40 μM; Figure 1B and Suppl. Figure 1). These data identify KNX-002 as a
128 potentially specific inhibitor of *T. gondii* class XIVa myosin activity.

129 **KNX-002 inhibits the growth of *T. gondii* in cell culture, with no detectable toxicity to human**
130 **cells.** The three lipid bilayers that comprise the pellicle of *T. gondii, i.e.*, the plasma membrane and
131 subjacent double bilayer of the inner membrane complex [34, 35], represent a potential barrier to the
132 penetration of externally applied drugs. To determine if KNX-002 can access and inhibit the motor in live
133 parasites, we determined the compound's effect on parasite expansion in culture in a modified plate-
134 based growth assay (see Methods and ref. [36]). KNX-002 does indeed inhibit parasite growth, in a dose-
135 dependent manner (Figure 2A), with an IC_{50} of 16.2 μM (95% confidence interval [C.I.] 13.0 - 20.5 μM;
136 Figure 2B).

137 Parasite growth in culture involves repeated lytic cycles comprised of host cell invasion, intracellular
138 replication, lysis of and egress from the infected cell, and migration to new host cells. While invasion,
139 egress and migration are all TgMyoA-dependent processes, intracellular replication does not require
140 TgMyoA [26, 28]. To test whether any portion of the observed growth inhibition in culture is due to off-
141 target effect(s) of KNX-002 on parasite replication, we scored the number of parasites per
142 parasitophorous vacuole over time during the lytic cycle. The compound had no detectable effect on
143 parasite replication in this assay (Suppl. Figure 2).

144 To exclude the possibility that the effect of KNX-002 on parasite growth was due to a deleterious
145 effect on the host cells, we also tested the effect of the compound on human foreskin fibroblasts (the
146 host cells used in the growth assays) and human HepG2 liver cells (sensitive indicators of cytotoxicity
147 and genotoxicity [37]) in 72-hour multiplexed cytotoxicity and cellular viability assays. KNX-002 showed
148 no detectable deleterious effect on either cell line in either assay at the highest concentration tested (80
149 μM; Figure 2C).

150 **Structure-activity relationship (SAR) analysis**. Next, we used the ATPase and parasite growth
151 assays to carry out a preliminary SAR study, with the goal of determining which parts of KNX-002 are
152 important for its biological activity. We began by modifying the *p*-OMe substituted aryl ring in KNX-002
153 (colored red in KNX-002 structure, Figure 3). Replacement of this structural unit in full by a hydrogen

154 atom (in **VEST1**) confirmed the importance of this part of the molecule for biological activity (Figure 3 and
155 Suppl. Figures 3 and 4). In terms of the preferred substituent on this aryl ring, inhibition of both *in vitro*
156 ATPase activity and parasite growth were retained when the *p*-OMe substituent in KNX-002 was
157 replaced by *p*-Cl (**VEST2**), and partially retained in analogs containing *p*-Me (**VEST3**) or *m*,*p*-dichloro
158 (**VEST4**) substituents. **VEST5**, an analog in which the *p*-OMe in KNX-002 was replaced by a hydrogen,
159 was significantly less active than KNX-002 in the purified protein assay but a strong inhibitor of parasite
160 growth. **VEST5** was not toxic to host cells, extracellular parasites, or intracellular parasites (Suppl.
161 Figures 5 and 6); further studies will be required to understand the activity of this analog in the parasite
162 growth assay. The mild to moderate toxicity levels shown by **VEST2** (*p*-Cl) against HepG2 and HFF cells,
163 compared to the lack of toxicity in either cell line demonstrated by KNX-002, led to the preliminary
164 conclusion that the *p*-OMe aryl substituent present in the starting KNX-002 analogue was preferred.
165 A series of additional analogs containing the *p*-OMe aryl substituent were also assessed.
166 Substitution of the thiophene ring in KNX-002 for a phenyl ring (in **VEST6,** highlighted in blue, Figure 3A)
167 led to a drop in activity in both the *in vitro* ATPase and growth inhibition assays. However, the retention
168 of some biological activity by **VEST6** may provide a way to assess rapidly the importance of additional
169 substitution in this region of the molecule in future studies through the incorporation of substituents on
170 the new phenyl ring. No tolerance for replacement of the pyrazole (highlighted in green) and thiophene
171 (blue) rings in KNX-002 was observed, with analogs containing only a phenyl, thiazole or furan
172 substituent, instead of the thiophene-linked pyrazole, all being inactive in both assays (**VEST7**, **VEST8**
173 and **VEST9**). Substitution of a pyrrole into KNX-002 to give **VEST10** led to loss of activity in the *in vitro*
174 assay but retention of some activity in the growth inhibition assay. Finally, the importance of the
175 cyclopropyl group in KNX-002 (highlighted in purple, Figure 3A) was confirmed by the lack of biological
176 activity in either assay of the *des*-cyclopropyl analog **VEST11**. The growth inhibition activity associated
177 with **VEST5** was also shown to require the cyclopropyl group as analogs **VEST12** (CH_2,) and **VEST13**
178 (CMe_2) were both less active in the growth assay. Attempts to incorporate a stereogenic center through
179 the replacement of the cyclopropyl group with a single methyl substituent led to analogs with decreased
180 biological activity and mild cytotoxicity against HFF cells (**VEST14** and **VEST15**).
181 These preliminary studies have identified regions of KNX-002 important for its biological activity,
182 which will inform subsequent efforts at compound optimization (see Discussion). Since no analogs with
183 higher potency than KNX-002 were identified in this first round of SAR analysis, all experiments reported
184 below were carried out using KNX-002.
185 **KNX-002 inhibits parasite motility.** To test whether KNX-002 inhibits parasite motility, we first
186 used a standard immunofluorescence-based assay that visualizes the protein "trails" left behind the
187 parasites as they glide on a glass coverslip (*e.g.*, [38, 39]). Untreated parasites deposit a variety of
188 helical, meandering, and large diameter circular trails in this qualitative two-dimensional assay (Figure
189 4A). Treatment with 10 μM KNX-002 results in a markedly different motility pattern, consisting almost
190 entirely of small diameter circles, and 25 μM KNX-002 dramatically inhibits the number of parasites
191 undergoing any movement at all (Figure 4A).

192 To more quantitatively evaluate differences in parasite motility in the presence of KNX-002, we used
193 a 3D motility assay that automatically analyzes thousands of trajectories in a single experiment, providing
194 robust statistical comparisons between populations of parasites [16, 21]. KNX-002 treatment decreases
195 the fraction of the parasite population moving in the 3D assay in a dose-dependent manner (Figures 4B
196 and 4C; IC_{50} = 5.3 μM, 95% C.I. 3.1- 7.8 μM). Of those parasites that move, KNX-002 treatment also
197 reduces their average displacement and speed (Suppl. Figure 7).
198 **Identification of a mutation in TgMyoA that confers partial resistance to KNX-002.** The results
199 presented thus far show that KNX-002 is an inhibitor of TgMyoA activity, parasite growth in culture, and
200 parasite motility. The data do not, however, directly link the compound's effects on parasite motility and
201 growth to inhibition of TgMyoA function; it remains possible that the inhibition of parasite motility and
202 growth are due to off-target effect(s). As a first step towards validating the specificity of the compound,
203 we chemically mutagenized parasites with N-ethyl-N-nitrosourea [40] and selected for parasites resistant
204 to KNX-002 by growth in 40 μM KNX-002. Parasites that grew up after 10-14 days under selection were
205 cloned and their sensitivity to KNX-002 determined using the plate-based growth assay. We isolated 26
206 such clones from two independent mutagenesis/selection experiments, five of which showed at least a
207 2.5-fold increase in IC_{50} for KNX-002 (Suppl. Figure 8). cDNA was generated from the five clones, and
208 each of the motor constituents (TgMyoA, TgMLC1, TgELC1 and TgELC2) was sequenced. Four of the
209 five resistant clones contained no amino acid-altering mutations in the motor genes; the fifth (clone R3)
210 contained a single A to G point mutation in the coding sequence of TgMyoA that changes threonine130
211 to alanine (T130A). This clone showed a 2.9-fold increase in IC_{50} for KNX-002 in the growth assay
212 (Figure 5A,B), from 14.9 μM (wildtype; 95% C.I. = 10.2 to 22.6 μM) to 43.4 μM (T130A mutant; 95% C.I.
213 = 37.0 to 51.2 μM). T130 is highly conserved in eukaryotic myosins (Figure 5C) and located on the first of
214 seven β-strands comprising the transducer subdomain (Figure 5D). The residues immediately flanking
215 T130 are also well conserved between the MyoA homologs of other apicomplexan parasites, but diverge
216 in the vertebrate myosins examined (Figure 5C).
217 To independently establish that the T130A mutation alters the sensitivity of TgMyoA to KNX-002, we
218 expressed recombinant TgMyoA containing the T130A mutation and compared its motion-generating
219 capacity to that of wild-type TgMyoA in an *in vitro* motility assay that measures the speed with which
220 fluorescently labeled actin filaments are moved by myosin adsorbed to a glass coverslip [20, 41]. In the
221 absence of added compound, the wild-type motor moved 92.5± 1.2% of the filaments on the coverslip,
222 with an average mean speed of 4.6 ± 0.3 μm/sec (Figure 6A, top and middle panels, grey bars). The
223 T130A mutation had no effect on the fraction of filaments moving in the assay, but decreased the basal
224 speed of filament sliding by 77 ± 3% compared to wild-type (Figure 6B, top and middle panels, grey
225 bars). Accordingly, we tested whether the mutant was misfolded, prone to aggregation, or otherwise
226 unstable by comparing its size-exclusion chromatography (SEC) elution profile and thermal stability, as
227 measured by differential scanning fluorimetry (DSF), to that of the wild-type motor (Suppl. Figure 9; both
228 proteins assayed in the near-rigor [SEC] and pre-powerstroke [DSF] states). No mutation-associated

229 differences were seen in either assay, suggesting that the effects of the T130A mutation on motor
230 function are not due to large structural changes in the protein caused by the amino acid substitution.
231 Including KNX-002 in the *in vitro* motility assay with wild-type motor inhibits both the fraction of actin
232 filaments moving and the speed of those filaments that do move, each in a dose-dependent manner
233 (Figure 6A, top and middle panels). Combining these two effects into a single "filament motility index"
234 (*i.e.*, the fraction of filaments moving multiplied by the mean speed of the filaments that do move)
235 provides a better measure of the overall effect of the compound in the assay. KNX-002 induces a large
236 decrease in the filament motility index (Figure 6A, bottom panel).
237 In marked contrast to the wild-type motor, KNX-002 had little to no effect on the fraction of actin
238 filaments moved by the motor containing the T130A mutation (Figure 6B, top panel). Furthermore,
239 although the basal filament sliding speed of the mutant motor was lower than that of wildtype, this
240 reduced sliding speed was also insensitive to compound (Figure 6B, middle panel), as was the mutant
241 motor's overall filament motility index (Figure 6B, bottom panel).
242 Taken together, these data confirm that the T130A mutation renders TgMyoA less sensitive to the
243 inhibitory effects of KNX-002.
244 **Validation of the specificity of KNX-002 in parasites.** The resistant parasite line generated by
245 mutagenesis and selection (clone R3, Figure 5B) is expected to contain as many as 70 different
246 mutations throughout its genome [40] in addition to the T130A mutation. To confirm that resistance to
247 KNX-002 in this parasite line was due to the identified mutation in TgMyoA, we recreated the single
248 T130A mutation in the wild-type background using CRISPR/Cas9 (Suppl. Figure 10). To quantitatively
249 evaluate effects of the mutation on the parasite's lytic cycle, we compared wild-type and T130A parasites
250 in a plaque assay, which encompasses the parasite's entire lytic cycle. The T130A mutation had no
251 significant effect on the number of plaques formed or plaque area (Suppl. Figure 11A, B), demonstrating
252 little to no effect of the mutation on the parasite's lytic cycle or growth in culture. Consistent with the
253 plaque assay results, the T130A mutation also had little to no effect on the fraction of the parasite
254 population moving in the 3D motility assay (compare the leftmost pair of panels in Figure 7A and two sets
255 of grey bars in Figure 7B) and only a minor effect on their mean trajectory speeds (compare the two sets
256 of grey bars, Figure 7C). Finally, the T130A mutation had no detectable effect on the virulence of the
257 parasite in a mouse model of infection (Suppl. Figure 11C).
258 We next asked whether parasites expressing the T130A mutation were less sensitive to KNX-002 in
259 the 3D motility assay). As shown above (Figure 4C), KNX-002 strongly inhibits the fraction of wild-type
260 parasites that move in Matrigel (Figure 7B, left three sets of bars). In contrast, the fraction of T130A
261 parasites that move during the assay was insensitive to KNX-002, up to concentrations of 20 μM (Figure
262 7B, right three sets of bars). The parasite speed data are more variable (Figure 7C and Suppl. Figure 7B)
263 but show that the mutant parasites retain some sensitivity to the compound (Figure 7C, right three sets of
264 bars). To capture the combined impact of changes to these two motility parameters and to facilitate
265 comparison to the *in vitro* motility results with recombinant motor, we calculated the "parasite motility
266 index" (the fraction of parasites moving multiplied by the average speed of those that do move) under

267 each condition. The wild-type parasite motility index is more severely impacted by KNX-002 treatment
268 than the motility index of T130A parasites (Figure 7D).
269 The displacement of both wild-type and mutant parasites is also inhibited by KNX-002 (Suppl. Figure
270 7A and Suppl. Figure 12), but the mutants are again less sensitive to the compound, *i.e.*, despite moving
271 shorter distances in the absence of compound (compare the two sets of grey bars in Suppl. Figure 12),
272 the T130A parasites moved farther than wildtype in the presence of 20 μM KNX-002 (compare the third
273 and sixth bars in Suppl. Figure 12). The decreased sensitivity of the T130A parasites to the effects of
274 KNX-002 is apparent in the maximum intensity projections from the 3D motility assay, which show more
275 T130A parasites than wildtype moving in the presence of 20 μM KNX-002, with longer average
276 displacements (compare right two sets of panels in Figure 7A).
277 Plaque assays were used to compare the growth of wildtype and mutant parasites in culture in the
278 presence of KNX-002. Parasites expressing the mutant motor formed a significantly larger number of
279 plaques in the presence of 20 μM compound than wild-type parasites, and even at 40 μM KNX-002 the
280 mutant parasites were still able to generate small plaques (Figure 8).
281 These data demonstrate that the T130A mutation confers partial resistance to the compound's
282 effects on motor function, parasite motility and parasite growth, confirming that TgMyoA is a biologically
283 relevant target for KNX-002 in *T. gondii*.
284 **KNX-002 treatment slows disease progression in mice infected with a lethal dose of *T. gondii*,**
285 **through a specific effect on TgMyoA.** Finally, we tested whether KNX-002 (20mg/kg, administered
286 intraperitoneally on the day of infection and two days later) can alter the progression of disease in a
287 mouse model of infection. Only 20% of the mice that were infected with wild-type parasites and treated
288 with vehicle were still alive 8 days post-infection, and none survived to day 9 (Figure 9, top panel, black
289 circles). In marked contrast, 90% of the mice treated with KNX-002 survived to day 8, 80% to day 9, and
290 40% were still alive on day 11 when the experiment was terminated (Figure 9, top panel, orange
291 squares).
292 When the same experiment was done with parasites expressing the T130A mutant myosin, the
293 vehicle-treated mice did not survive beyond day 8 (Figure 9, bottom panel, black circles), similar to what
294 we observed with wild-type parasites. Critically, and in marked contrast to infection with wild-type
295 parasites, KNX-002 treatment did not significantly improve the survival of mice infected with the T130A
296 parasites (Figure 9, bottom panel, orange squares).
297 Together, these data show that KNX-002 can slow disease progression in mice infected with *T.*
298 *gondii*, and prove that the compound exerts its effects through inhibition of its intended target, TgMyoA.
299
300 **Discussion**
301
302 The intense interest in motility among those who study apicomplexan parasites reflects both the
303 unique nature of the process and its importance in parasite biology and virulence. These parasites move
304 without the cilia, flagella or protruding leading edge that drives the motility of most other eukaryotic cells.

305 The class XIV myosins clearly play a central role in motility, but they are unusual myosins in many
306 respects [17, 23], and precisely how these myosins and their interacting proteins function to drive motility
307 remains controversial [27, 42-47]. The mechanisms underlying motility are therefore of fundamental cell
308 biological interest. Since MyoA is essential for virulence, highly conserved in apicomplexan parasites,
309 and different in several respects from the myosins found in humans, the MyoA motor complex also
310 represents a potentially attractive target for drug development. We describe here the identification and
311 characterization of a novel small molecule, KNX-002, which will be a useful chemical probe for future
312 studies of the function of TgMyoA. Importantly, we also identified a mutation in TgMyoA that reduces the
313 sensitivity of the motor to KNX-002. We used isogenic parasites lines expressing either the wild-type or
314 mutant myosin to unequivocally demonstrate that TgMyoA is a biologically relevant target of the
315 compound in parasites and to show that pharmacological inhibition of TgMyoA can slow the progression
316 of disease in mice infected with a lethal dose of *T. gondii*.

317 **KNX-002 as a chemical probe for studying class XIV motor function.** Most previous studies of
318 TgMyoA motor function involved phenotypic characterization of parasites in which the genes encoding
319 TgMyoA or its associated proteins were either disrupted or their expression downregulated (*e.g.*, [26, 27,
320 46, 48]). Such reverse genetic approaches, particularly gene disruptions, are powerful but blunt tools for
321 studying the mechanisms underlying processes important to parasite survival, such as motility.
322 Pharmacological inhibitors that interact specifically with a target of interest provide a useful
323 complementary approach for studying motility and other facets of parasite biology [49, 50], since different
324 aspects of the target's function can be perturbed at specific times and in a controlled manner. Because
325 the parasites are exposed to the compound for only short periods of time, compensatory adaptations
326 (*e.g.*, through mutation or changes in gene expression) that can confound data interpretation in
327 experiments involving gene disruption [31, 32] are unlikely to occur. Even experiments involving
328 controlled protein depletion or transcriptional downregulation of a gene of interest, which can be
329 achieved in hours to days, run the risk of inducing compensatory changes in transcription, translation,
330 protein stability, post-translational modifications, or the localization of proteins with overlapping function
331 (*e.g.*, [30-32]). Determining the effect of a pharmacological inhibitor of motility can, in contrast, be
332 accomplished within minutes (*e.g.,* Figures 4, 7).

333 There have been only two previously reported attempts to pharmacologically manipulate the function
334 of TgMyoA. In the first, the general myosin inhibitor 2,3-butanedione monoxime (BDM) was shown to
335 inhibit parasite motility [38]; however, BDM is now recognized as an inhibitor with so many off-target
336 effects that little can be concluded from its use in cells [51, 52]. The other study used computational
337 methods and a homology model of TgMLC1 bound to TgMyoA to identify two predicted inhibitors of
338 TgMLC1-TgMyoA interaction [53]. These two compounds (C3-20 and C3-21) inhibit *T. gondii* growth with
339 sub-micromolar IC_{50}s [53] but whether this effect on parasite growth is due to inhibition of TgMyoA has
340 not been established.

341 The compound we have identified and characterized here, KNX-002, inhibits the ability of
342 recombinant TgMyoA to propel actin filaments in the *in vitro* motility assay, and decreases the speed of

343 the filaments that move (Figure 6A). Similar effects are seen in the 3D motility assay: compound
344 treatment reduces both the number of parasites moving and, to a lesser extent, the speeds with which
345 these parasites move (Figure 7B, C and Suppl. Figure 7B). To provide a better picture of the combined
346 impact of changes to these two motility parameters, we multiplied the fraction of actin filaments or
347 parasites moving by the mean actin filament/parasite speed to generate the filament/parasite motility
348 index. In the *in vitro* motility assay with wild-type TgMyoA, fraction moving and speed contributed
349 approximately equally to the filament motility index in both the presence and absence of the compound.
350 In wild-type parasites, the compound-induced changes to fraction moving are larger than to speed and
351 therefore the predominant contributor to the changes in parasite motility index upon compound
352 treatment. Precisely how the effects of the compound on motor function in the *in vitro* motility assay
353 relate to the observed changes in parasite motility will require further study. Nevertheless, the data
354 presented demonstrate the value of KNX-002 as a new chemical probe for studying the mechanism(s)
355 underlying the unusual form of eukaryotic cell motility used by *T. gondii*.
356 Excitingly, KNX-002 and a recently discovered analog named KNX-115 were shown to inhibit
357 PfMyoA, the TgMyoA homolog of the malaria parasite, *P. falciparum* [54, 55], and to block the growth of
358 blood stage *P. falciparum* in culture and the invasion of hepatocytes by liver stage parasites [54, 55].
359 Structure-function studies revealed that the compound sequesters PfMyoA in a state of low affinity for
360 actin [54], consistent with a decrease in duty ratio we observe in wild-type TgMyoA treated with KNX-002
361 (Suppl. Figure 13).
362 **Effects of the T130A mutation.** The T130A mutation that confers partial resistance to KNX-002
363 was identified by chemical mutagenesis and selection in KNX-002. While the mutagenesis/selection
364 approach is commonly used to generate resistant parasites in *T. gondii* and other apicomplexan
365 parasites (*e.g.*, [56-58]), the next step after isolating resistant clones is typically to do whole genome
366 sequencing on the most promising of the resistant clones to identify potentially relevant mutations. We
367 took a more direct and scalable approach in this study, by sequencing only the motor protein loci
368 (TgMyoA, TgMLC1, TgELC1, TgELC2) in the resistant parasites, since (a) the goal of this study was to
369 identify a direct inhibitor of motor function, and (b) we had already shown that KNX-002 can inhibit the
370 activity of recombinant motor consisting only of TgMyoA, TgMLC1, and TgELC1 (note: since TgELC1
371 and TgELC2 are functionally redundant [19], a mutation in the gene encoding either could confer
372 compound resistance). Of the five resistant clones whose IC_{50} for KNX-002 shifted 2.5-fold or more
373 relative to wildtype in the growth assay, only one had a mutation in the coding sequence of one of the
374 motor protein genes, T130A in TgMyoA. The source of resistance in the other four clones is unknown.
375 T130, which lies in the first β-strand at the extreme N-terminus of the transducer domain [24], is not
376 predicted to be directly involved in the binding of KNX-002 [54], even though other aspects of the
377 transducer may be involved [54]. Thus, the mechanism by which the T130A mutation confers partial
378 resistance to the compound is likely to be indirect. For example, the T130A mutation could induce long
379 range structural changes that alter the KNX-002 binding pocket, thereby mitigating the effect of the
380 compound. However, myosin motors depend on a complex and highly interconnected network of

381 allosteric interactions to perform their function [59], making it difficult to predict precisely how the T130A
382 mutation reduces the sensitivity of TgMyoA to KNX-002.
383 While the T130A mutation reduces the sensitivity of the motor to KNX-002, the mutation is not
384 without its effects on motor performance, causing a 75-80% reduction in basal filament sliding speed in
385 the *in vitro* motility assay (Figure 6B). However, when expressed in parasites the mutation had a much
386 less pronounced effect on parasite motility (compare the first and fourth sets of grey bars in Figures 7B-
387 D). We explored several possible explanations for this differential effect of the T130A mutation on the
388 activity of the recombinant motor *vs.* motor-driven motility of the parasites. First, the mutation might alter
389 the folding or stability – and therefore the activity – of the recombinant TgMyoA used in the *in vitro*
390 assays. This seems unlikely, since the mutant motor was indistinguishable from the wild-type motor by
391 SEC and DSF (Suppl. Figure 9). Second, the partially functional motor might be overexpressed in the
392 mutant parasites. This possibility was ruled out by quantitative western blotting (Suppl. Figure 14A).
393 Third, the parasite might compensate for the loss of TgMyoA activity in the T130A mutants through
394 changes in the transcription of other myosins, myosin light chains, glideosome components, actin or actin
395 regulatory proteins. No such changes to known motility-associated proteins were observed by RNAseq
396 analysis (Suppl. Figure 14B, right panel). Furthermore, analysis of all differentially regulated transcripts
397 revealed that 57% of the genes up/down regulated more than log2-fold were annotated as hypothetical
398 proteins, and the remainder were largely associated with trafficking and metabolism (Suppl. Figure 14B,
399 left panel) so cannot readily explain a compensation mechanism in parasites with impaired motor
400 function, although further studies would be required to definitively rule out this possibility. The compound
401 might have less of an effect on motor function in the parasite due to some protein or factor present in the
402 parasite (but not the insect cell system used to produce recombinant motor) that can counteract the
403 deleterious effects of the mutation. Alternatively, the density of TgMyoA motors might be higher in the
404 parasite pellicle than on the glass coverslips used in the *in vitro* motility assays, and therefore require
405 higher concentrations of compound to achieve equivalent levels of inhibition. Regardless of the reason
406 for this differential impact of the mutation on *in vitro* and parasite motility, it is notable that the fraction of
407 actin filaments moving *in vitro* and the fraction of parasites moving within Matrigel were better correlated
408 than the speeds of actin filament and parasite movement. The fraction of filaments moving in the *in vitro*
409 motility assay may therefore be more relevant to motor-driven parasite motility than filament sliding
410 speed.
411 The mutagenesis protocol used to generate the T130A mutation kills 70% of the initial parasite
412 population and results in an average of 63 mutations per parasite across the genome [40]. It is unclear
413 how these harsh experimental mutagenesis conditions relate to what occurs during a natural infection
414 and therefore how readily parasites showing reduced sensitivity to KNX-002 (or, more likely, an
415 optimized compound based on the KNX-002 scaffold) would arise during treatment of a human infection.
416 From the drug development perspective, it would be useful to know what other resistance mechanisms
417 are available to the parasite for this class of compounds. Further characterization of the four partially
418 resistant mutants identified here that have no mutations in the TgMyoA motor (Suppl. Figure 8) would be

419 a good place to start. TgMyoA knockout parasites are still capable of a small degree of 3D motility (13%
420 of wild-type levels [46] under the same assay conditions used here). Although controversial [46], it has
421 been proposed that TgMyoC can to some extent functionally compensate for the loss of TgMyoA [30,
422 31], so mutations in TgMyoC would be of particular interest. It should be noted that because humans are
423 a dead-end host for *Toxoplasma*, even if resistance were to emerge within a treated individual through
424 mutations in TgMyoA or some other locus in the genome, the chances of this resistance spreading
425 human-to-human or into the zoonotic reservoir are exceedingly small.

426 **MyoA as a druggable target.** A few small molecule inhibitors of mammalian myosins have shown
427 potential as therapeutics (reviewed in [51]). The most well characterized myosin inhibitor is blebbistatin, a
428 noncompetitive inhibitor of myosin II [60]. Blebbistatin has been a useful chemical probe for studying
429 myosin II function [51], and derivatives are being considered for cancer chemotherapy [61, 62] and drug
430 addiction [63]. A more recently discovered inhibitor, MYK-461 (mavacamten), decreases the duty ratio of
431 cardiac muscle myosin through an effect on P_i release, reduces the development of ventricular
432 hypertrophy in a mouse model of hypertrophic cardiomyopathy (HCM; [64]), and has been approved by
433 the FDA for use in the treatment of hypertrophic cardiomyopathy patients.

434 The MyoA motor complex of apicomplexan parasites has long been considered an attractive target
435 for drug development [25, 33, 53, 65-67]. However, no previous studies have tested whether small
436 molecule inhibitors of TgMyoA or other apicomplexan myosins can alter the course of infection *in vivo*.
437 The argument against MyoA as a drug target has been that the parasite may have alternative and/or
438 compensatory mechanisms to enable motility in the absence of MyoA [26, 27, 43, 45, 46], meaning that
439 simultaneous inhibition of more than one motility pathway may be necessary to provide sufficient
440 protection against infection. However, *T. gondii* engineered to express low levels of TgMyoA, which may
441 be more analogous to drug-treated parasites than a knockout, are completely avirulent [28], arguing that
442 sufficiently strong inhibition of TgMyoA is likely, on its own, to be therapeutically useful.

443 Given this rationale, a major motivation behind the work reported here was to develop the tools
444 necessary to rigorously test whether MyoA can be targeted by small molecules to alter the course of an
445 infection. We demonstrated that it is possible to identify small molecules that inhibit parasite TgMyoA,
446 have no detectable effect on vertebrate myosins, and show no toxicity to mammalian cells. Furthermore,
447 one of these compounds, KNX-002, was shown to be capable of inhibiting myosin function in the
448 parasite, thereby disrupting parasite motility and the lytic cycle. The specificity of KNX-002 for TgMyoA in
449 these experiments was demonstrated using parasites expressing the T130A mutation, and the
450 observation that treatment with KNX-002 decreases the susceptibility of mice to a lethal infection with
451 wild-type, but not T130A parasites, proves that TgMyoA is indeed a druggable target, *in vivo*. Whether
452 KNX-002 can also inhibit the activity of any of the parasite's other ten myosins [68] and disrupt their
453 biological function(s) will be the subject of future study.

454 While KNX-002 provided the means to rigorously test the druggability of TgMyoA, it caused weight
455 loss and histological evidence of liver damage in the treated infected mice. Before further animal work, it

456 will therefore be necessary to develop more potent and less toxic analogs that retain specificity for
457 parasite myosin. Our preliminary SAR data (summarized in Figure 3) are consistent with a key role for
458 the pyrazole, cyclopropyl, and *p*-OMe aryl units within KNX-002, with a generally good correlation
459 between the results of the recombinant myosin ATPase and parasite growth inhibition assays.
460 Subsequent studies, inspired both by our SAR data and the recently reported structure of the PfMyoA-
461 KNX-002 complex [54], could explore the effect on biological activity of: (i) alternative replacements for
462 the thiophene group and (ii) a switch in the positions of the NH and CH_2 groups, amongst other options.
463 Encouragingly, Trivedi *et al* recently identified an analog of KNX-002 that shows >20-fold improved
464 potency against recombinant PfMyoA [55]. Although neither the structure of this analog nor the SAR
465 strategy that led to its discovery were disclosed, this result suggests there is considerable opportunity to
466 optimize the biological properties of the KNX-002 scaffold through a systematic SAR campaign.
467 KNX-002 and any improved analogs developed through further rounds of iterative SAR will be useful
468 new experimental tools for studying the role of MyoA in parasite growth, dissemination and virulence,
469 and provide an exciting opportunity to develop an entirely new class of drugs that can be used to prevent
470 or treat the severe diseases caused by *T. gondii* and other apicomplexan parasites.
471
472 **Methods**
473
474 **Cell and parasite culture.** Parasites were propagated by serial passage in human foreskin fibroblasts
475 (HFFs). HFFs were grown to confluence in Dulbecco's Modified Eagle's Medium (DMEM) (Life
476 Technologies, Carlsbad, CA) containing 10% v/v heat-inactivated fetal bovine serum (FBS) (Life
477 Technologies, Carlsbad, CA), 10 mM HEPES pH 7, and 100 units/ml penicillin and 100 µg/ml
478 streptomycin, as previously described [69]. Prior to infection with *T. gondii*, the medium was changed to
479 DMEM supplemented with 10mM HEPES pH 7, 100 units/ml penicillin and 100 µg/ml streptomycin, and
480 1% v/v FBS.
481
482 **Compounds.** KNX-002 was either obtained commercially from Asinex (Winston-Salem NC; Figures 1,
483 2, 4-8 and S1, S2, S6-S8, S11-13) or synthesized, purified and characterized as described below
484 (Figures 3, 9 and S3-5, S10). The commercially sourced and in-house synthesized compounds had
485 similar IC_{50}s in parasite growth assays: see IC_{50} values and overlapping 95% confidence intervals in
486 Figures 2 and 5 (commercial) and Figure 3 (synthesized). Compounds were dissolved in dimethyl
487 sulfoxide (DMSO) and stored at -20ºC, in the dark, until use. In all experiments involving treatment with
488 compound, an equivalent amount of DMSO was added to all samples in that experiment, including the
489 DMSO only vehicle controls. Final concentrations of DMSO were 0.5% v/v for experiments with
490 recombinant TgMyoA, 0.1% v/v for experiments with parasites and cells, and 34 µl DMSO per injection
491 per 20g mouse for the *in vivo* experiments.
492

493 **High-throughput screen.** Compound CK2140597 was originally identified through high-throughput
494 screening of a library of 50000 compounds (40uM final concentration, 2% v/v DMSO), performed by JS
495 and EW at Cytokinetics, Inc., to identify inhibitors of the actin-activated ATPase of TgMyoA, provided by
496 AK and GEW. The same compounds were screened, in parallel, against *Plasmodium falciparum* MyoA
497 (PfMyoA; protein provided by Kathy Trybus, University of Vermont). The assay used was a coupled
498 enzymatic assay [70]. Actin was first polymerized using 1 mM ATP, 2 mM $MgCl_2$, 20 mM KCl and left on
499 ice for 30 minutes. Buffer A was made with PM12 (12 mM Pipes-KOH, pH 7.0, 2 mM $MgCl_2$), 1mM DTT,
500 0.1 mg/ml BSA, 0.4 mM PK/LDH, 1 µg/ml TgMyoA, 0.009% v/v Anitfoam (Millipore Sigma, St. Louis MO).
501 Buffer B was made with PM12, 1 mM DTT, 0.1 mg/ml BSA, 1 mM ATP, 1 mM NADH, 1.5 mM PEP, 0.6
502 mg/ml previously polymerized actin and 0.009% v/v Antifoam. 12.5 µl of each buffer were added to a
503 plate with a Packard MiniTrak liquid handler and then mixed at 2400 for 45 seconds with an BioShake
504 3000 ELM orbital plate mixer (Qinstruments). The decrease in optical density at 340 nm as a function of
505 time was measured on an Envision 2104 spectrophotometer (Perkin Elmer) with a 600 s data monitoring
506 window sampled every 60 s. Hit progression included confirmation of activity in an independent
507 experiment, inactivity against an unrelated ATPase (hexokinase from Millipore Sigma), and dose-
508 responsive inhibition. Hexokinase reactions were performed using glucose (1 mM) and sufficient
509 hexokinase to generate ADP from ATP at a rate similar to the target myosins. Based on pre-established
510 thresholds, CK2140597 was identified as a hit in the TgMyoA but not the PfMyoA screen; however,
511 resupplied compound was subsequently shown to also be active against PfMyoA by Trybus and
512 colleagues. CK2140597 was licensed by Kainomyx (www.kainomyx.com), renamed KNX-002, and
513 released for academic studies in the laboratory of GEW (for *Toxoplasma*) and Kathy Trybus
514 (for *Plasmodium*).
515
516 **Vertebrate myosin ATPase assays.** Myofibril preparations from striated muscles are a well-established
517 model for assaying myosin ATPase activity in a semi-native context [71]. Bovine cardiac, rabbit fast
518 skeletal, and bovine masseter slow skeletal myofibrils were prepared and assayed as previously
519 described [72], except they were tested at 75% calcium activation (pCa75) since this high level of basal
520 ATPase activity enables the sensitive detection of inhibitors. For smooth muscle myosin (SMM), native
521 chicken gizzard SMM S1 was prepared, crosslinked to bovine cardiac actin using EDC/NHS, and
522 assayed as previously described [73].
523
524 **Expression and purification of recombinant TgMyoA.** TgMyoA was co-expressed with TgMLC1,
525 TgELC1, and TgUNC in Sf9 cells and purified as previously described [33]. TgMyoA containing the
526 T130A mutation was generated using the QuikChange II-Site-Directed Mutagenesis method (Agilent
527 Scientific, Santa Clara CA) . Briefly, mutant strand synthesis was performed by denaturing baculovirus
528 plasmid pSmTgMyoAcBiocfFLAG, annealing primers P21 and P22 (Table 1), which contain the desired
529 mutation and using PfuUltra high fidelity taq polymerase in a thermocycling reaction to incorporate and
530 extend the primer product. The product was then digested by DpnI overnight at 37 °C and the resulting

531 plasmid was purified using a Qiagen PCR purification kit. Subsequently, the purified PCR product was
532 used to transform electro-competent DH5-alpha cells. Positive clones were screened, plasmid prepped
533 and the presence of the mutation verified by sequencing.
534
535 ***In vitro* motility.** *in vitro* motility assays with chicken skeletal muscle actin were performed as previously
536 described [33] with the following modifications: (a) Neutravidin (40 ug/ml, Molecular Probes) in buffer B
537 was added to the flow cells first, followed by BSA (in buffer B) and 3 washes with buffer B; (b)
538 approximately 0.16 µg of FLAG purified TgMyoA was used per flow cell; (c) Buffer C was in all cases
539 supplemented with oxygen scavengers (3 mg/ml glucose (Sigma-Aldrich), 0.125 mg/ml glucose oxidase
540 (Sigma-Aldrich), and 0.05 mg/ml catalase (Sigma-Aldrich); (d) All washes with Buffer C were done 3
541 times; and (e) bacterially expressed TgEMLC1 and TgELC1 were each added to the flow cells at a
542 concentration of 25 µg/ml. Data were collected on an Eclipse Ti-U inverted microscope (Nikon) equipped
543 with a 100× Plan Apo objective lens (1.49 NA) and a XR/Turbo-Z camera (Stanford Photonics) running
544 Piper Control software (v2.3.39). Data were collected at 10 frames per second. Actin filament tracking
545 and analysis was done in Imaris ×64 v. 7.6.1 (Bitplane AG, Zurich, Switzerland).
546
547 **Duty ratio measurements.** To compare the duty cycle of WT recombinant TgMyoA with and without
548 KNX-002 treatment, the number of myosin heads capable of interacting with an actin filament was
549 estimated as described previously [20, 74]. Briefly, the *in vitro* motility assay was carried out as described
550 above using various concentrations of myosin treated with either 10 µM KNX-002 or the equivalent
551 amount (0.5% v/v) of DMSO. At each concentrations of myosin on the coverslip, actin filament length
552 and velocity was measured in Imaris ×64 v. 7.6.1 (Bitplane AG, Zurich, Switzerland) and an estimate of
553 the number of heads available to interact with an actin filament was determined. Duty cycle (f) were
554 calculated by plotting filament velocity (V) against number of heads (N). These data were then fit to the
555 equation $V = (a \times V_{max}) \times [1-(1-f)^n]$ by non-linear regression analysis (GraphPad Prism (Version 9.4.0
556 (453)) as previously described [74, 75].
557
558 **Parasite growth assays.** Fluorescence-based growth assay. To quantify growth in the presence of
559 compound(s), $1x10^4$ tachyzoites were preincubated with compound for 5 minutes prior to inoculation onto
560 3 wells of a black sided, clear bottom 384-well plate containing a confluent monolayer of HFF cells. For
561 compound assays, parasites expressing tdTomato were incubated with vehicle or serial dilutions of
562 compound, maintaining a constant DMSO concentration (0.2% v/v). The fluorescent signal was
563 quantified daily for 7 days (ex 530/25, em 590/35) on a Biotek synergy 2 plate reader. The IC_{50} of growth
564 inhibitory compounds was quantified using GraphPad Prism. Plaque assay. 10, 100, 200, or 500
565 parasites were used to inoculate a confluent monolayer of HFF cells in a 12-well plate and incubated for
566 7 days at 37ºC, 5% CO_2. Infected monolayers were then washed with phosphate-buffered saline, fixed
567 with 100% EtOH for five minutes, stained with 5X crystal violet solution (12.5 g crystal violet, 125 ml
568 100% EtOH, 500 ml 1% w/v ammonium oxalate) for 5 minutes, washed with PBS, and allowed to dry.

569 Wells were imaged using BioTek ImmunoSpot S6 MACRO Analyzer, and plaque number and area were
570 measured using the Analyze Particles tools in Fiji v2.3.0.
571
572 **Parasite motility assays.**
573 2D motility assays were performed as previously described [76], using monoclonal antibody DG52
574 (generously provided by Dr. David Sibley) against TgSAG1 for immunofluorescent staining of the trails.
575 3D motility assays were performed as previously described [16]. Briefly, parasites were syringed
576 released and filtered using a 3-µm Whatman Nuclepore filter (Millipore Sigma) before spinning and
577 resuspending in motility buffer containing 0.5 mg/ml Hoechst 33342. A mixture of 1:3:3 of parasites,
578 motility buffer with compound, and Matrigel was created and pipetted into a flow cell. Flow cells were
579 incubated for 7 minutes at 27ºC and then 3 minutes at 35ºC. Images were captured using a Nikon
580 Eclipse TE300 epifluorescence microscope (Nikon Instruments, Melville, NY) using a 20× PlanApo λ
581 objective and a NanoScanZ piezo Z stage insert (Prior Scientific, Rockland, MA). For the data shown in
582 Figures 4B,C and Suppl. Figure 7, an iXON 885 EMCCD camera (Andor Technology, Belfast, Ireland)
583 driven by NIS Elements software v. 3.20 (Nikon Instruments, Melville, NY) was used to collect time lapse
584 image (502 pixel × 500 pixel) stacks of the fluorescently label parasite nuclei, with Mercury lamp
585 excitation. Images were captured for 60 sec. The camera was set to trigger mode, 2×2 binning, readout
586 speed of 35 MHz, conversion gain of 3.8x, and EM gain setting of 3. For the data shown in Figure 7 and
587 Suppl. Figure 12, 1024 pixel × 384 pixel images were captured using an iXON Life 888 EMCCD camera
588 (Andor Technology) driven by NIS Elements software v.5.11, including the Illumination Sequence
589 acquisition module (Nikon Instruments), and excited using a pE-4000 LED illumination system (CoolLED,
590 Andover England). Images were captured for 80 sec. The camera was set to trigger mode, no binning,
591 readout speed of 30 Mhz, conversion gain of 3.8x, and an EM gain of 300.
592 All motility assays captured image stacks consisting of 41 z-slices, captured 1 um apart with a 16ms
593 exposure time. The data were analyzed using Imaris ×64 v. 9.2.0 (Bitplane AG, Zurich, Switzerland). The
594 ImarisTrack module tracked the parasite nuclei using an estimated spot volume of 3.0 × 3.0 × 6.0 µm. A
595 maximum distance of 6.0 µm and maximum gap size of 2 were applied to the tracking algorithm. A track
596 duration filter of 10 seconds was used to avoid tracking artifacts and a 2 µm displacement filter was used
597 to eliminate parasites moving by Brownian motion [16].
598
599 **Mutagenesis and selection for resistant parasites.** The dose of ENU required to kill 70% of parasites
600 [40] during a 4 hour treatment was determined by plaque assay (see above). For each mutagenesis,
601 tdTomato-expressing parasites were liberated from large vacuoles by scraping the monolayer and
602 syringe release through a 26G needle, then treated with ENU at the 70% kill concentration for 4 hours.
603 The parasites were washed 3x in DMEM containing 1% v/v fetal bovine serum to remove residual ENU
604 and inoculated onto a T25 of confluent HFF cells. 24 - 48h post infection, surviving parasites that had
605 lysed their host cells were transferred to fresh HFF cells and grown for until plaques became visible (10-
606 14 days) in the presence of 40 µM KNX-002, which is close to the compound's estimated EC_{90} value in

607 the growth assay (37.6μM; 95% C.I. 18.9-136.4 μM). Clonal lines were isolated by serial dilution in five
608 96-well plates per mutagenesis. Parasite sensitivity to KNX-002 was then determined by fluorescence-
609 based growth assay (see above).
610 RNA was isolated from resistant clones with the GeneJET RNA purification kit and used to generate
611 cDNA with the Agilent cDNA synthase kit for oligoDT synthesis. cDNA encoding TgMyoA, TgMLC1,
612 TgELC1, TgELC2 was amplified and sequenced with primers covering the entire transcript (Table 1, P6-
613 P20). Sequence alignments were analyzed in SnapGene and sequences containing non-synonymous
614 mutations were compared to other strains to identify naturally occurring polymorphisms unlikely to be
615 responsible for resistance.
616
617 **Generation of TgMyoA T130A mutant using CRISPR/Cas9.** All oligonucleotides were synthesized by
618 Sigma-Aldrich (The Woodlands, TX), and restriction enzymes were purchased from New England
619 Biolabs (Ipswich, MA). To generate the Cas9eGFPTgMyoAguide plasmid (Suppl. Figure 10), plasmid
620 pSAG1::Cas9-U6::sgUPRT [77] was PCR amplified with primers P1 and P2 (Table 1). This linear
621 pSAG1::Cas9-U6::sgUPRT PCR product contained all features of the original vector, the TgMyoA T130
622 protospacer sequence (5'-GAATCAGATCTACGCGACTG-3'), and introduced an EcoRI site. The T130A
623 double stranded repair template was produced by annealing oligonucleotides P3 and P4 (Table 1). This
624 repair template contains the T130A mutation and two additional mutations that do not alter the amino
625 acid sequence: a mutation introducing a diagnostic BglII site and a mutation ablating the PAM sequence
626 (Suppl. Figure 10A). RHΔku80Δhxgprt parasites were transfected with the ds repair template and
627 Cas9eGFPTgMyoAguide plasmid (Suppl. Figure 10B). Wild-type RHΔku80Δhxgprt and transfected
628 tachyzoites were syringe released and filtered 2 days post-transfection. eGFP+ parasites were sorted 3-
629 per well onto a 96-well plate in the UVM Flow Cytometry and Cell Sorting Facility using a FACSAria cell
630 sorter (Becton Dickinson Biosciences, Franklin Lakes NJ). Positive clonal populations were validated for
631 GFP expression 7 days post-sorting.
632 To identify T130A positive mutant clones, gDNA was purified from WT and transfected parasites
633 directly from 96-well plates using previously methods [78]. PCR fragments of approximately the first 3kb
634 of MyoA were generated using the Phire tissue direct PCR Master kit (Thermo Fisher Scientific, Waltham
635 MA) with primers P5 and P11 (Table 1). Diagnostic digests with BglII provided an initial screen for T130A
636 mutant parasites as the ds repair template introduced a third BglII site into the amplified sequence
637 (Suppl. Figure 10C). Positive T130A mutant clones were further verified by harvesting tachyzoite cDNA
638 and sequencing using primers P5-P13 (Table 1).

639 **Western Blotting.** Protein samples were resolved by SDS–polyacrylamide gel electrophoresis and
640 transferred to Immobilon®-FL polyvinylidene fluoride membrane (Millipore Sigma) as previously
641 described [76]. Blots were probed with rabbit anti-TgMyoA antiserum UVT109 (diluted 1:1000) and rabbit
642 anti-TgACT1 (1:10,000; generous gift from Dr. David Sibley). Goat anti-rabbit IRDye800CW (1:20,000;

643 LI-COR Biosciences, Lincoln, NE) was used as a secondary antibody. The blots were scanned using an
644 Odyssey CLx infrared imager (LI-COR) and analyzed using Image Studio software v.2.1.10 (LI-COR).

645 **Mammalian cell toxicity assays.** HFF and HepG2 cells were grown to ~80% confluence in 384-well
646 plates before media was replaced with DMEM containing 10% v/v fetal bovine serum and serial dilutions
647 of compound or vehicle while maintaining a consistent DMSO concentration (0.2% v/v). Cells were
648 incubated with compound at 37℃ for 72h before multiplexed quantitation of toxicity using CellTox
649 green™ and cell viability using Cell-TiterGlo® (both assay kits from Promega Corp, Madison WI). As a
650 positive control for toxicity 24h prior to cessation of the assay 0.5 mM NaN_3 was added to half of the
651 vehicle wells to induce cell death. CellTox green**.** To quantify dead, dying and damaged cells in each
652 well, an equal volume (25µl) of CellTox green reagent (1:500 CellTox green dye in CellTox green assay
653 buffer) was added to each well and mixed on an orbital shaker (700 - 900rpm) for 1 minute. The plate
654 was equilibrated at room temperature for 15 minutes before quantifying the fluorescence signal (ex
655 485/20, em 528/20) using a Biotek Synergy 2 plate reader. CellTiter-Glo. Following quantification of
656 toxicity, the number of viable cells/well was quantified by adding 25µl CellTiter-Glo reagent to each well.
657 To maximize cell lysis plates were mixed on an orbital shaker (700 - 900rpm) for 5 minutes before
658 equilibration at room temperature for an additional 10 minutes. Quantitation was achieved by measuring
659 luminescence per well using a Biotek Synergy 2 plate reader.

660 **Parasite replication assay.** Confluent HFF monolayers grown in clear bottomed black-sided 96-well
661 plates were challenged with $1x10^4$ tachyzoites and incubated for 1 hour at 37°C with 5% CO_2.
662 Monolayers were then washed once with DMEM containing 1% v/v fetal bovine serum before incubating
663 with 0 (DMSO vehicle only) or compound. Monolayers were fixed with 2% v/v PFA 12h, 24h and 36h
664 after compound addition. After blocking and permeabilization in 0.2% v/v Triton X-100 and 1% w/v bovine
665 serum albumin, samples were incubated with Mab 45.36 against TgIMC1 for 2 hours (3.7 µg/ml) at 23ºC.
666 Monolayers were washed three times with blocking buffer before incubation in the dark with a 1:1000
667 dilution of Alexa546-conjugated anti-rabbit IgG (ThermoFisher) for 1 hour at 23ºC. The number in
668 parasites in each of 50 vacuoles per sample were counted blind.

669 **Parasite toxicity assays.** Extracellular parasite toxicity**.** $1x10^7$ parasites in DMEM containing 1% v/v
670 fetal bovine serum were mixed in a 96-well plate with 0 (DMSO vehicle only), 40, or 80µM KNX-002, in a
671 final volume of 50µl. The plate was incubated for 1 or 3 hours at 37°C with 5% CO_2. 50µl CellTiter-Glo
672 reagent was added to each well and mixed on an orbital shaker for 5 minutes (500 – 700rpm), followed
673 by a 15-minute incubation at 23ºC. The relative number of viable parasites was quantified by
674 luminescence, read on a Biotek Synergy 2 plate reader. Intracellular parasite toxicity in the presence of
675 various concentrations of compound was determined using the replication assay described above.

676 **ATPase assays.** ATPase assays for the SAR studies were performed per manufacturer's
677 recommendations using the ADP-Glo Kinase Assay (Promega Corp, Madison WI). Briefly, 8 µl kinase

678 reactions were performed by combining 5 µl of myosin (0.128 mg/ml), 1 µl of actin (4.8 mg/ml), 1 µl of
679 ATP (8 mM) and 1 µl of 1X Kinase Reaction Buffer (40 mM Tris pH 7.6, 20 mM $MgCl_2$, and 0.1 mg/ml
680 BSA). After a 90 minute incubation at room temperature, 5 ul of ADP-Glo Reagent was added to the
681 kinase reaction followed by a 40 minute incubation at room temperature. Finally, 10 ul of Kinase
682 Detection Reagent was added and after a 60 minute incubation, ATP production was detected by
683 measuring luminescence with a Synergy H1 Hybrid plate reader. For compound inhibitor experiments,
684 the control reactions contained 0.5% v/v DMSO and compounds were diluted in 1X Kinase Reaction
685 Buffer. All assays were performed under conditions where ADP generation (measured in relative
686 luminescence units, RLU) was linear with respect to both TgMyoA concentration and incubation time.
687 Reactions were performed in duplicate on each plate and all experiments were replicated three times.
688 Data were analyzed using GraphPad Prism.
689
690 **Size-exclusion Chromatography.** Twin-strep-II (TST)-tagged TgMyoA (1-778) (ToxoDB ID
691 TGGT1_070410/GenBank™ accession number EPR60343.1) wild-type and T130A mutant were
692 expressed in *Trichoplusia ni* (Tni) insect cells. Protein was purified by streptactin affinity, and finally SEC,
693 using a final buffer containing 20 mM HEPES pH 7.5, 150 mM NaCl, and 1 mM DTT. Prior to DSF
694 experiments, purified, concentrated TgMyoA (1-778) was diluted with buffer containing $MgCl_2$, ADP, NaF,
695 and $Al(NO_3)_3$, to final concentrations of 2 mM $MgCl_2$, 2 mM ADP, 6 mM NaF, 1.75 mM $Al(NO_3)_3$.
696
697 **Differential Scanning Fluorimetry.** Purified TgMyoA (1-778) WT and T130A were diluted to 1.0 mg/mL
698 in buffer containing 150 mM NaCl; 20mM HEPES, pH 7.5; 1 mM $MgCl_2$; 1 mM ADP; 6 mM NaF; 1.75 mM
699 $Al(NO_3)_3$; 1 mM DTT; and SYPRO® orange dye at a final concentration of 5X. 20 µL reactions were
700 tested in triplicate using the StepOnePlus™ Real-Time PCR System from ThermoFisher, with all
701 replicate samples obtained from a single preparation of MyoA protein.
702
703 **Mouse infections.** Infections were carried out in 4-5 week old male CBA/J mice purchased from
704 Jackson Laboratories. All mice were socially housed and acclimated for 3 days prior to infections. For
705 virulence studies a total of nine mice (three biological replicates of three mice each) were challenged by
706 intraperitoneal injection of either 50 or 1000 wild-type (RH) or T130A parasites resuspended in a total
707 volume of 200µl sterile PBS. Daily animal health monitoring began two days after infection. Mice were
708 euthanized when predetermined welfare thresholds were exceeded.
709 For KNX-002 treatment studies, 15 mice were injected intraperitoneally with either 20mg/kg KNX-
710 002 (40mM compound stock in DMSO diluted into PBS containing 30% v/v polyethylene glycol 400) or
711 an equivalent amount of DMSO (vehicle) in the same diluent. 20-30 minutes after compound/vehicle
712 injection, ten compound-treated mice were intraperitoneally infected with either 500 wild-type or 500
713 T130A mutant parasites, and five vehicle-treated mice were similarly infected with either wild-type or
714 T130A mutant parasites. A second intraperitoneal injection of 20mg/kg KNX-002 or DMSO was given two
715 days later. The rationale for this dosing schedule was two-fold: (a) We expected the compound to work

716 primarily on egressing and extracellular parasites. Since the parasite's lytic cycle takes approximately 48
717 hours, this two-day injection schedule was chosen to maximize exposure of the extracellular parasites to
718 freshly injected compound early in establishment of the infection. (b) A preliminary KNX-002 dose
719 tolerance study was conducted prior to the infection experiments. Two doses of 20mg/kg (the highest
720 dose tested) administered two days apart revealed minor hepatoxicity without signs of excessive pain or
721 distress and was therefore considered the maximal tolerated dose.
722 Daily animal health monitoring began two days after infection, and mice were euthanized when
723 predetermined welfare thresholds were exceeded. All animal experiments were carried out under
724 University of Vermont Institutional Animal Care and Use Committee protocol #PROTO202000126.
725
726 **RNA sequencing.** For each sample, three confluent flasks of HFFs cells were inoculated with either
727 wild-type or T130A mutant parasites. Two days after infection, when vacuoles were large (≳64
728 parasites/vacuole), parasites were harvested by scraping the flask and passing the suspension three
729 times through a 26G needle. Released parasites were incubated at 37ºC for 1 hr, and RNA was then
730 isolated using the GeneJET RNA Purification kit (Thermo-Fisher) following manufacturer instructions. For
731 each sample, 1µg of total RNA (A260/280 = 1.8-2.2, A260/230 ≥ 1.8) was sent to Novogene for library
732 preparation and sequencing to a read depth of 20 million paired end reads per sample. Quality control
733 and sequence alignment to the *Toxoplasma* genome (toxodb.org) was done in house. The most
734 differentially expressed genes were identified from all genes expressed in all samples, with a FPKM >
735 0.1 and an adjusted p-value of < 0.05. Expression of known TgMyoA interacting proteins, glideosome
736 components, actin and actin regulatory factors were also separately quantified where detected in all
737 three replicates of both the wildtype and T130A mutant. TgELC2 (TGME49_305050) was not
738 consistently expressed and therefore was excluded from the analysis shown in Suppl. Figure 14.

739 **Compound synthesis and characterization.** Details of compound synthesis and analysis are
740 presented in Supplementary Data. Mass spectroscopic (m/z) data were obtained by Mrs. Caroline
741 Horsburgh at the University of St Andrews mass spectrometry service. Electrospray ionization
742 techniques were applied and a ThermoFisher LTQ Orbitrap XL spectrometer was used. Values are
743 quoted as a ratio of mass to charge (m/z) in Daltons [Da]. NMR spectra were recorded on either a Bruker
744 Ascend 500 (^{1}H 600; ^{13}C 150 MHz) or a Bruker Advance II 400 (^{1}H 400; ^{13}C 101 MHz). ^{13}C NMR spectra
745 were taken with a DEPTQ pulse sequence. Spectra were recorded using deuterated solvents. For ^{1}H
746 NMR analysis, multiplicities of signals are denoted as follows: s (singlet), d (doublet), t (triplet), q
747 (quartet), dd (doublet of doublets), dt (doublet of triplets), m (multiplet). Coupling constants (J) are quoted
748 to the nearest 0.1 Hz. Chemical shifts (δ) are stated in ppm and referenced to residual solvent signals
749 ($CHCl_3$ 7.260 ppm (s), 77.160 ppm (t); $(CD_3)_2SO$ 2.50 ppm (s) or 39.52 ppm (pentet)). IR spectra were
750 obtained using a Shimadzu IRAffinity 1S IR Spectrometer as ATR. The IR data were processed using
751 OriginPro 2022 v9.9.0.225. Optical rotations were determined using a Perkin Elmer Model 341

752 Polarimeter with a Na/Hal lamp (Na D line, 589 nm). Melting points were measured using capillary tubes
753 on an Electrothermal 9100 melting point apparatus. Values are quoted in ranges and to 1.0 °C.

754

755 **Acknowledgements**

756 This work was supported by U.S. Public Health Service (USPHS) grants AI139201 and AI137767 (GEW)
757 and GM141743 (DMW), and by Canadian Institutes of Health Research Grant 148596 (MJB), as well as
758 fellowships from the USPHS (F31AI145214; RVS) and American Heart Association (20POST35220017;
759 RSK). AS was supported by USPHS training grant T32AI055402. MJB gratefully acknowledges the
760 Canada Research Chair program for salary support. We thank Cytokinetics, Inc., for their willingness to
761 provide staff time and reagents to this project, Samantha Previs for technical support, Dr. Shane Nelson
762 for help with the duty ratio analysis, and Dr. Roxanna del Rio-Guerra for her flow cytometry advice and
763 assistance. Genomic-scale data sets and ancillary information were obtained from the Toxoplasma
764 Genome Database (ToxoDB.org). ToxoDB is a component of the Eukaryotic Pathogen, Vector and Host
765 Informatics Resource [79], supported by the National Institutes of Allergy and Infectious Diseases and
766 the Wellcome Trust; we gratefully acknowledge the staff responsible for developing and maintaining this
767 resource.

768 The authors declare that they have no conflicts of interest.

769 **References**

770 1. Dubey JP, Murata FHA, Cerqueira-Cézar CK, Kwok OCH, Villena I. Congenital toxoplasmosis in
771 humans: an update of worldwide rate of congenital infections. Parasitology. 2021:1-11. Epub
772 2021/07/14. doi: 10.1017/s0031182021001013. PubMed PMID: 34254575.

773 2. El Bissati K, Levigne P, Lykins J, Adlaoui EB, Barkat A, Berraho A, et al. Global initiative for
774 congenital toxoplasmosis: an observational and international comparative clinical analysis. Emerg
775 Microbes Infect. 2018;7(1):165. Epub 2018/09/29. doi: 10.1038/s41426-018-0164-4. PubMed
776 PMID: 30262847; PubMed Central PMCID: PMCPMC6160433.

777 3. Vidal JE, Hernandez AV, de Oliveira AC, Dauar RF, Barbosa SP, Jr., Focaccia R. Cerebral
778 toxoplasmosis in HIV-positive patients in Brazil: clinical features and predictors of treatment
779 response in the HAART era. AIDS Patient Care STDS. 2005;19(10):626-34. Epub 2005/10/20. doi:
780 10.1089/apc.2005.19.626. PubMed PMID: 16232047.

781 4. Porter SB, Sande MA. Toxoplasmosis of the central nervous system in the acquired
782 immunodeficiency syndrome. N Engl J Med. 1992;327(23):1643-8. Epub 1992/12/03. doi:
783 10.1056/NEJM199212033272306. PubMed PMID: 1359410.

784 5. de Oliveira GB, da Silva MA, Wanderley LB, da Cunha Correia C, Ferreira EC, de Medeiros ZM, et
785 al. Cerebral toxoplasmosis in patients with acquired immune deficiency syndrome in the
786 neurological emergency department of a tertiary hospital. Clin Neurol Neurosurg. 2016;150:23-6.
787 doi: 10.1016/j.clineuro.2016.08.014. PubMed PMID: 27573702.

788 6. Gandhi RT. Toxoplasmosis in HIV-infected patients. UpToDate. 2015.

789 7. http://www.unaids.org/en/resources/documents/2017/UNAIDS_FactSheet. Fact Sheet - Latest
790 Global and Regional Statistics on the Status of the AIDS Epidemic Communications and Global
791 Advocacy [Internet]. 2017 July 20, 2017.

792 8. Ben-Harari RR, Goodwin E, Casoy J. Adverse Event Profile of Pyrimethamine-Based Therapy in
793 Toxoplasmosis: A Systematic Review. Drugs R D. 2017;17(4):523-44. doi: 10.1007/s40268-017-
794 0206-8. PubMed PMID: 28879584; PubMed Central PMCID: PMCPMC5694419.

795 9. Choquet-Kastylevsky G, Vial T, Descotes J. Allergic adverse reactions to sulfonamides. Curr
796 Allergy Asthma Rep. 2002;2(1):16-25. PubMed PMID: 11895621.

797 10. McLeod R, Khan AR, Noble GA, Latkany P, Jalbrzikowski J, Boyer K, et al. Severe sulfadiazine
798 hypersensitivity in a child with reactivated congenital toxoplasmic chorioretinitis. Pediatr Infect Dis
799 J. 2006;25(3):270-2. doi: 10.1097/01.inf.0000202070.59190.9a. PubMed PMID: 16511396.

800 11. McPhillie M, Zhou Y, El Bissati K, Dubey J, Lorenzi H, Capper M, et al. New paradigms for
801 understanding and step changes in treating active and chronic, persistent apicomplexan infections.
802 Scientific reports. 2016;6:29179. doi: 10.1038/srep29179. PubMed PMID: 27412848; PubMed
803 Central PMCID: PMCPMC4944145.

804 12. Barragan A, Sibley LD. Transepithelial migration of *Toxoplasma gondii* is linked to parasite motility
805 and virulence. J Exp Med. 2002;195(12):1625-33. PubMed PMID: 12070289.

806 13. Furtado JM, Bharadwaj AS, Ashander LM, Olivas A, Smith JR. Migration of *Toxoplasma gondii*-
807 infected dendritic cells across human retinal vascular endothelium. Invest Ophthalmol Vis Sci.
808 2012;53(11):6856-62. Epub 2012/09/07. doi: 10.1167/iovs.12-10384. PubMed PMID: 22952125;
809 PubMed Central PMCID: PMC3466064.

810 14. Sibley LD. Intracellular parasite invasion strategies. Science. 2004;304(5668):248-53. PubMed
811 PMID: 15073368.

812 15. Harker KS, Ueno N, Lodoen MB. *Toxoplasma gondii* Dissemination: A Parasite's Journey through
813 the Infected Host. Parasite Immunol. 2015;37:141-9. Epub 2014/11/20. doi: 10.1111/pim.12163.
814 PubMed PMID: 25408224.

815 16. Leung JM, Rould MA, Konradt C, Hunter CA, Ward GE. Disruption of *TgPHIL1* alters specific
816 parameters of *Toxoplasma gondii* motility measured in a quantitative, three-dimensional live motility
817 assay. PLOS One. 2014;9(1):e85763. Epub 2014/02/04. doi: 10.1371/journal.pone.0085763.
818 PubMed PMID: 24489670; PubMed Central PMCID: PMC3906025.

819 17. Herm-Gotz A, Weiss S, Stratmann R, Fujita-Becker S, Ruff C, Meyhofer E, et al. *Toxoplasma*
820 *gondii* myosin A and its light chain: a fast, single-headed, plus-end-directed motor. EMBO J.
821 2002;21(9):2149-58.

822 18. Nebl T, Prieto JH, Kapp E, Smith BJ, Williams MJ, Yates JR, 3rd, et al. Quantitative *in vivo*
823 analyses reveal calcium-dependent phosphorylation sites and identifies a novel component of the
824 *Toxoplasma* invasion motor complex. PLOS Pathog. 2011;7(9):e1002222. PubMed PMID:
825 21980283.

826 19. Williams MJ, Alonso H, Enciso M, Egarter S, Sheiner L, Meissner M, et al. Two Essential Light
827 Chains Regulate the MyoA Lever Arm To Promote *Toxoplasma* Gliding Motility. MBio. 2015;6(5).
828 Epub 2015/09/17. doi: 10.1128/mBio.00845-15. PubMed PMID: 26374117.

829 20. Heaslip AT, Leung JM, Carey KL, Catti F, Warshaw DM, Westwood NJ, et al. A small-molecule
830 inhibitor of *T. gondii* motility induces the posttranslational modification of myosin light chain-1 and
831 inhibits myosin motor activity. PLOS Pathog. 2010;6(1):e1000720. doi:
832 10.1371/journal.ppat.1000720. PubMed PMID: 20084115.

833 21. Leung JM, Tran F, Pathak RB, Poupart S, Heaslip A, Ballif BA, et al. Identification of *T. gondii*
834 myosin light chain-1 as a direct target of tachypleginA-2, a small-molecule inhibitor of parasite

835 motility and invasion. PLOS One. 2014;9(6):e98056. doi: 10.1371/journal.pone.0098056. PubMed
836 Central PMCID: PMC4043638.

837 22. Bement WM, Mooseker MS. TEDS rule: a molecular rationale for differential regulation of myosins
838 by phosphorylation of the heavy chain head. Cell Motil Cytoskeleton. 1995;31(2):87-92. Epub
839 1995/01/01. doi: 10.1002/cm.970310202. PubMed PMID: 7553910.

840 23. Heintzelman MB, Schwartzman JD. A novel class of unconventional myosins from *Toxoplasma*
841 *gondii*. J Mol Biol. 1997;271(1):139-46.

842 24. Powell CJ, Ramaswamy R, Kelsen A, Hamelin DJ, Warshaw DM, Bosch J, et al. Structural and
843 mechanistic insights into the function of the unconventional class XIV myosin MyoA from
844 Toxoplasma gondii. Proc Natl Acad Sci U S A. 2018;115(45):E10548-e55. Epub 2018/10/24. doi:
845 10.1073/pnas.1811167115. PubMed PMID: 30348763; PubMed Central PMCID:
846 PMCPMC6233092.

847 25. Trivedi DV, Nag S, Spudich A, Ruppel KM, Spudich JA. The Myosin Family of Mechanoenzymes:
848 From Mechanisms to Therapeutic Approaches. Annu Rev Biochem. 2020;89:667-93. Epub
849 2020/03/15. doi: 10.1146/annurev-biochem-011520-105234. PubMed PMID: 32169021.

850 26. Egarter S, Andenmatten N, Jackson AJ, Whitelaw JA, Pall G, Black JA, et al. The *Toxoplasma*
851 Acto-MyoA motor complex is important but not essential for gliding motility and host cell invasion.
852 PLOS One. 2014;9(3):e91819. Epub 2014/03/19. doi: 10.1371/journal.pone.0091819. PubMed
853 PMID: 24632839; PubMed Central PMCID: PMC3954763.

854 27. Andenmatten N, Egarter S, Jackson AJ, Jullien N, Herman JP, Meissner M. Conditional genome
855 engineering in *Toxoplasma gondii* uncovers alternative invasion mechanisms. Nat Methods.
856 2012;10(2):125-7. Epub 2012/12/25. doi: 10.1038/nmeth.2301. PubMed PMID: 23263690; PubMed
857 Central PMCID: PMC3605914.

858 28. Meissner M, Schluter D, Soldati D. Role of *Toxoplasma gondii* myosin A in powering parasite
859 gliding and host cell invasion. Science. 2002;298(5594):837-40. PubMed PMID: 12399593.

860 29. Bichet M, Touquet B, Gonzalez V, Florent I, Meissner M, Tardieux I. Genetic impairment of parasite
861 myosin motors uncovers the contribution of host cell membrane dynamics to *Toxoplasma* invasion
862 forces. BMC biology. 2016;14(1):97. doi: 10.1186/s12915-016-0316-8. PubMed PMID: 27829452;
863 PubMed Central PMCID: PMCPMC5101828.

864 30. Frenal K, Marq JB, Jacot D, Polonais V, Soldati-Favre D. Plasticity between MyoC- and MyoA-
865 glideosomes: an example of functional compensation in *Toxoplasma gondii* invasion. PLOS
866 Pathog. 2014;10(10):e1004504. Epub 2014/11/14. doi: 10.1371/journal.ppat.1004504. PubMed
867 PMID: 25393004; PubMed Central PMCID: PMC4231161.

868 31. Frenal K, Soldati-Favre D. Plasticity and Redundancy in Proteins Important for *Toxoplasma*
869 Invasion. PLOS Pathog. 2015;11(8):e1005069. Epub 2015/08/14. doi:
870 10.1371/journal.ppat.1005069. PubMed PMID: 26270966; PubMed Central PMCID: PMC4536160.

871 32. Lamarque MH, Roques M, Kong-Hap M, Tonkin ML, Rugarabamu G, Marq JB, et al. Plasticity and
872 redundancy among AMA-RON pairs ensure host cell entry of *Toxoplasma* parasites. Nat Commun.
873 2014;5:4098. Epub 2014/06/18. doi: 10.1038/ncomms5098. PubMed PMID: 24934579.

874 33. Bookwalter CS, Kelsen A, Leung JM, Ward GE, Trybus KM. A *Toxoplasma gondii* class XIV
875 myosin, expressed in Sf9 with a parasite co-chaperone, requires two light chains for fast motility. J
876 Biol Chem. 2014;289(44):30832-41. doi: 10.1074/jbc.M114.572453.

877 34. Harding CR, Meissner M. The inner membrane complex through development of *Toxoplasma*
878 *gondii* and *Plasmodium*. Cell Microbiol. 2014;16(5):632-41. Epub 2014/03/13. doi:
879 10.1111/cmi.12285. PubMed PMID: 24612102.

880 35. Kono M, Prusty D, Parkinson J, Gilberger TW. The apicomplexan inner membrane complex. Front
881 Biosci (Landmark Ed). 2013;18:982-92. Epub 2013/06/12. PubMed PMID: 23747861.

882 36. Gubbels MJ, Li C, Striepen B. High-Throughput Growth Assay for *Toxoplasma gondii* Using Yellow
883 Fluorescent Protein. Antimicrob Agents Chemother. 2003;47(1):309-16. PubMed PMID: 12499207.

884 37. Mersch-Sundermann V, Knasmüller S, Wu XJ, Darroudi F, Kassie F. Use of a human-derived liver
885 cell line for the detection of cytoprotective, antigenotoxic and cogenotoxic agents. Toxicology.
886 2004;198(1-3):329-40. Epub 2004/05/13. doi: 10.1016/j.tox.2004.02.009. PubMed PMID:
887 15138059.

888 38. Dobrowolski JM, Carruthers VB, Sibley LD. Participation of myosin in gliding motility and host cell
889 invasion by *Toxoplasma gondii*. Mol Microbiol. 1997;26(1):163-73.

890 39. Hakansson S, Morisaki H, Heuser J, Sibley LD. Time-lapse video microscopy of gliding motility in
891 *Toxoplasma gondii* reveals a novel, biphasic mechanism of cell locomotion. Mol Biol Cell.
892 1999;10(11):3539-47.

893 40. Farrell A, Coleman BI, Benenati B, Brown KM, Blader IJ, Marth GT, et al. Whole genome profiling
894 of spontaneous and chemically induced mutations in *Toxoplasma gondii*. BMC Genomics.
895 2014;15:354. Epub 2014/06/03. doi: 10.1186/1471-2164-15-354. PubMed PMID: 24885922;
896 PubMed Central PMCID: PMC4035079.

897 41. Work SS, Warshaw DM. Computer-assisted tracking of actin filament motility. Anal Biochem.
898 1992;202(2):275-85. PubMed PMID: 1519753.

899 42. Gras S, Jimenez-Ruiz E, Klinger CM, Schneider K, Klingl A, Lemgruber L, et al. An endocytic-
900 secretory cycle participates in Toxoplasma gondii in motility. PLOS Biol. 2019;17(6):e3000060.
901 Epub 2019/06/25. doi: 10.1371/journal.pbio.3000060. PubMed PMID: 31233488.

902 43. Meissner M, Ferguson DJ, Frischknecht F. Invasion factors of apicomplexan parasites: essential or
903 redundant? Curr Opin Microbiol. 2013;16(4):438-44. Epub 2013/06/04. doi:
904 10.1016/j.mib.2013.05.002. PubMed PMID: 23727286.

905 44. Rompikuntal PK, Kent RS, Foe IT, Deng B, Bogyo M, Ward GE. Blocking Palmitoylation of
906 Toxoplasma gondii Myosin Light Chain 1 Disrupts Glideosome Composition but Has Little Impact
907 on Parasite Motility. mSphere. 2021;6(3). Epub 2021/05/21. doi: 10.1128/mSphere.00823-20.
908 PubMed PMID: 34011689.

909 45. Tardieux I, Baum J. Reassessing the mechanics of parasite motility and host-cell invasion. J Cell
910 Biol. 2016;214(5):507-15. doi: 10.1083/jcb.201605100. PubMed PMID: 27573462; PubMed Central
911 PMCID: PMCPMC5004448.

912 46. Whitelaw JA, Latorre-Barragan F, Gras S, Pall GS, Leung JM, Heaslip A, et al. Surface attachment,
913 promoted by the actomyosin system of *Toxoplasma gondii* is important for efficient gliding motility
914 and invasion. BMC biology. 2017;15(1):1. doi: 10.1186/s12915-016-0343-5. PubMed PMID:
915 28100223; PubMed Central PMCID: PMCPMC5242020.

916 47. Pavlou G, Touquet B, Vigetti L, Renesto P, Bougdour A, Debarre D, et al. Coupling Polar Adhesion
917 with Traction, Spring and Torque Forces Allows High Speed Helical Migration of the Protozoan
918 Parasite Toxoplasma. ACS nano. 2020;14:7121-39. Epub 2020/05/21. doi:
919 10.1021/acsnano.0c01893. PubMed PMID: 32432851.

920 48. Frenal K, Polonais V, Marq JB, Stratmann R, Limenitakis J, Soldati-Favre D. Functional dissection
921 of the apicomplexan glideosome molecular architecture. Cell Host Microbe. 2010;8(4):343-57.
922 PubMed PMID: 20951968.

923 49. Bogyo M, Ward GE. *Toxoplasma gondii* Chemical Biology. In: Weiss LM, Kim K, editors.
924 *Toxoplasma gondii* - The Model Apicomplexan: Perspectives and Methods. Second ed. London,
925 UK: Academic Press; 2014. p. 707-30.

926 50. Ward GE, Carey KL, Westwood NJ. Using small molecules to study big questions in cellular
927 microbiology. Cell Microbiol. 2002;4(8):471-82. doi: 10.1046/j.1462-5822.2002.00205.x. PubMed
928 PMID: 12174082.

929 51. Bond LM, Tumbarello DA, Kendrick-Jones J, Buss F. Small-molecule inhibitors of myosin proteins.
930 Future Med Chem. 2013;5(1):41-52. Epub 2012/12/22. doi: 10.4155/fmc.12.185. PubMed PMID:
931 23256812.

932 52. Ostap EM. 2,3-Butanedione monoxime (BDM) as a myosin inhibitor. J Muscle Res Cell Motil.
933 2002;23(4):305-8. PubMed PMID: 12630704.

934 53. Kortagere S, Mui E, McLeod R, Welsh WJ. Rapid discovery of inhibitors of *Toxoplasma gondii*
935 using hybrid structure-based computational approach. J Comput Aided Mol Des. 2011;25(5):403-
936 11. PubMed PMID: 21359560.

937 54. Moussaoui D, Robblee JP, Auguin D, Fisher F, Fagnant PM, Macfarlane JE, et al. Mechanism of
938 small molecule inhibition of Plasmodium falciparum myosin A informs antimalarial drug design.
939 bioRxiv. 2022:2022.09.09.507123. doi: 10.1101/2022.09.09.507123.

940 55. Trivedi DV, Karabina A, Bergnes G, Racca A, Wander H, Jung S, et al. A small-molecule myosin
941 inhibitor as a targeted multi-stage antimalarial. bioRxiv. 2022:2022.09.09.507317. doi:
942 10.1101/2022.09.09.507317.

943 56. Istvan ES, Dharia NV, Bopp SE, Gluzman I, Winzeler EA, Goldberg DE. Validation of isoleucine
944 utilization targets in *Plasmodium falciparum*. Proc Natl Acad Sci U S A. 2011;108(4):1627-32.
945 PubMed PMID: 21205898.

946 57. Rosenberg A, Luth MR, Winzeler EA, Behnke M, Sibley LD. Evolution of resistance in vitro reveals
947 mechanisms of artemisinin activity in Toxoplasma gondii. Proc Natl Acad Sci U S A. 2019. Epub
948 2019/12/07. doi: 10.1073/pnas.1914732116. PubMed PMID: 31806760.

949 58. Wu W, Herrera Z, Ebert D, Baska K, Cho SH, DeRisi JL, et al. A chemical rescue screen identifies
950 a Plasmodium falciparum apicoplast inhibitor targeting MEP isoprenoid precursor biosynthesis.
951 Antimicrob Agents Chemother. 2015;59(1):356-64. Epub 2014/11/05. doi: 10.1128/aac.03342-14.
952 PubMed PMID: 25367906; PubMed Central PMCID: PMCPMC4291372.

953 59. Preller M, Manstein DJ. Myosin structure, allostery, and mechano-chemistry. Structure.
954 2013;21(11):1911-22. Epub 2013/11/12. doi: 10.1016/j.str.2013.09.015. PubMed PMID: 24210227.

955 60. Allingham JS, Smith R, Rayment I. The structural basis of blebbistatin inhibition and specificity for
956 myosin II. Nat Struct Mol Biol. 2005;12(4):378-9. PubMed PMID: 15750603.

957 61. Duxbury MS, Ashley SW, Whang EE. Inhibition of pancreatic adenocarcinoma cellular invasiveness
958 by blebbistatin: a novel myosin II inhibitor. Biochem Biophys Res Commun. 2004;313(4):992-7.
959 PubMed PMID: 14706640.

960 62. Mikulich A, Kavaliauskiene S, Juzenas P. Blebbistatin, a myosin inhibitor, is phototoxic to human
961 cancer cells under exposure to blue light. Biochim Biophys Acta. 2012;1820(7):870-7. doi:
962 10.1016/j.bbagen.2012.04.003. PubMed PMID: 22507270.

963 63. Barkhuff WD, Gilk SD, Whitmarsh R, Tilley LD, Hunter C, Ward GE. Targeted disruption of *TgPhIL1*
964 in *Toxoplasma gondii* results in altered parasite morphology and fitness. PLOS One.
965 2011;6(8):e23977. Epub 2011/09/09. doi: 10.1371/journal.pone.0023977. PubMed PMID:
966 21901148; PubMed Central PMCID: PMC3162014.

967 64. Green EM, Wakimoto H, Anderson RL, Evanchik MJ, Gorham JM, Harrison BC, et al. A small-
968 molecule inhibitor of sarcomere contractility suppresses hypertrophic cardiomyopathy in mice.
969 Science. 2016;351(6273):617-21. doi: 10.1126/science.aad3456. PubMed PMID: 26912705;
970 PubMed Central PMCID: PMCPMC4784435.

971 65. Kortagere S, Welsh WJ, Morrisey JM, Daly T, Ejigiri I, Sinnis P, et al. Structure-based design of
972 novel small-molecule inhibitors of *Plasmodium falciparum*. J Chem Inf Model. 2010;50(5):840-9.
973 PubMed PMID: 20426475.

974 66. Bosch J, Turley S, Daly TM, Bogh SM, Villasmil ML, Roach C, et al. Structure of the MTIP-MyoA
975 complex, a key component of the malaria parasite invasion motor. Proc Natl Acad Sci U S A.
976 2006;103(13):4852-7. PubMed PMID: 16547135.

977 67. Thomas JC, Green JL, Howson RI, Simpson P, Moss DK, Martin SR, et al. Interaction and
978 dynamics of the *Plasmodium falciparum* MTIP-MyoA complex, a key component of the invasion
979 motor in the malaria parasite. Mol Biosyst. 2010;6(3):494-8. PubMed PMID: 20174678.

980 68. Mueller C, Graindorge A, Soldati-Favre D. Functions of myosin motors tailored for parasitism. Curr
981 Opin Microbiol. 2017;40:113-22. doi: 10.1016/j.mib.2017.11.003. PubMed PMID: 29161623.

982 69. Roos DS, Donald RG, Morrissette NS, Moulton AL. Molecular tools for genetic dissection of the
983 protozoan parasite *Toxoplasma gondii*. Methods in Cell Biology. 451994. p. 27-63.

984 70. Robert-Paganin J, Robblee JP, Auguin D, Blake TCA, Bookwalter CS, Krementsova EB, et al.
985 Plasmodium myosin A drives parasite invasion by an atypical force generating mechanism. Nat
986 Commun. 2019;10(1):3286. Epub 2019/07/25. doi: 10.1038/s41467-019-11120-0. PubMed PMID:
987 31337750; PubMed Central PMCID: PMCPMC6650474.

988 71. Lionne C, Iorga B, Candau R, Travers F. Why choose myofibrils to study muscle myosin ATPase?
989 J Muscle Res Cell Motil. 2003;24(2-3):139-48. Epub 2003/11/12. doi: 10.1023/a:1026045328949.
990 PubMed PMID: 14609025.

991 72. Hwee DT, Cheng AJ, Hartman JJ, Hinken AC, Lee K, Durham N, et al. The Ca(2+) sensitizer CK-
992 2066260 increases myofibrillar Ca(2+) sensitivity and submaximal force selectively in fast skeletal
993 muscle. J Physiol. 2017;595(5):1657-70. Epub 2016/11/22. doi: 10.1113/jp273248. PubMed PMID:
994 27869319; PubMed Central PMCID: PMCPMC5330873.

995 73. Sirigu S, Hartman JJ, Planelles-Herrero VJ, Ropars V, Clancy S, Wang X, et al. Highly selective
996 inhibition of myosin motors provides the basis of potential therapeutic application. Proc Natl Acad
997 Sci U S A. 2016;113(47):E7448-e55. Epub 2016/11/07. doi: 10.1073/pnas.1609342113. PubMed
998 PMID: 27815532; PubMed Central PMCID: PMCPMC5127359.

999 74. Harris DE, Warshaw DM. Smooth and skeletal muscle myosin both exhibit low duty cycles at zero
1000 load in vitro. J Biol Chem. 1993;268(20):14764-8. Epub 1993/07/15. PubMed PMID: 8325853.

1001 75. Walcott S, Fagnant PM, Trybus KM, Warshaw DM. Smooth muscle heavy meromyosin
1002 phosphorylated on one of its two heads supports force and motion. J Biol Chem.
1003 2009;284(27):18244-51. PubMed PMID: 19419961.

1004 76. Carey KL, Westwood NJ, Mitchison TJ, Ward GE. A small-molecule approach to studying invasive
1005 mechanisms of *Toxoplasma gondii*. Proc Natl Acad Sci U S A. 2004;101(19):7433-8. doi:
1006 10.1073/pnas.0307769101. PubMed PMID: 15123807.

1007 77. Shen B, Brown KM, Lee TD, Sibley LD. Efficient gene disruption in diverse strains of *Toxoplasma*
1008 *gondii* using CRISPR/CAS9. MBio. 2014;5(3):e01114-14. Epub 2014/05/16. doi:
1009 10.1128/mBio.01114-14. PubMed PMID: 24825012; PubMed Central PMCID: PMC4030483.

1010 78. Piro F, Carruthers VB, Di Cristina M. PCR Screening of Toxoplasma gondii Single Clones Directly
1011 from 96-Well Plates Without DNA Purification. Methods Mol Biol. 2020;2071:117-23. Epub
1012 2019/11/24. doi: 10.1007/978-1-4939-9857-9_6. PubMed PMID: 31758449.

1013 79. Amos B, Aurrecoechea C, Barba M, Barreto A, Basenko EY, Bażant W, et al. VEuPathDB: the
1014 eukaryotic pathogen, vector and host bioinformatics resource center. Nucleic Acids Res.
1015 2022;50(D1):D898-d911. Epub 2021/11/01. doi: 10.1093/nar/gkab929. PubMed PMID: 34718728;
1016 PubMed Central PMCID: PMCPMC8728164.

A

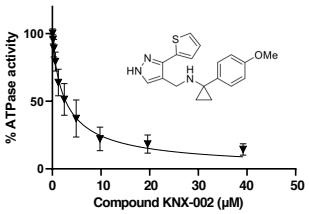

B

Test enzyme	IC_{50}	95% C.I.
TgMyoA	2.8 µM	2.4-3.2 µM
Chicken SMM	>39.2 µM	NA
Bovine cardiac myofibrils (pCa75)	>39.2 µM	NA
Rabbit fast skeletal myofibrils (pCa75)	>39.2 µM	NA
Bovine slow skeletal myofibrils (pCa75)	>39.2 µM	NA
Bovine slow skeletal myofibrils (pCa25)	>39.2 µM	NA
Hexokinase	>39.2 µM	NA

<u>Figure 1</u>: KNX-002 inhibits the actin-activated ATPase activity of TgMyoA but not vertebrate myosins. (A) The effect of various concentrations of KNX-002 on TgMyoA ATPase activity, normalized to the activity with an equivalent amount of DMSO (vehicle) only. Inset shows the structure of KNX-002. Each data point represents mean ATPase activity of three different batches of KNX-002 ± SEM. **(B)** The inhibitory effect of KNX-002 on TgMyoA and various vertebrate myosins (IC_{50} and 95% confidence interval [C.I.]). The dose-response curves for the individual vertebrate myosins are shown in Suppl. Figure 1.

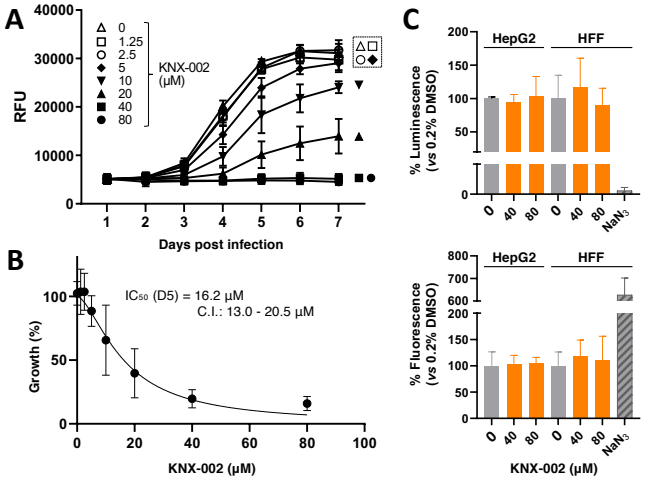

<u>Figure 2</u>: KNX-002 inhibits the growth of *T. gondii* in culture, with no detectable host cell toxicity. **(A)** tdTomato-expressing parasites were preincubated with various concentrations of KNX-002 for 5 minutes (0 = DMSO vehicle only) and then added to HFF cells on a 384-well plate. Fluorescence was measured daily to quantify parasite growth, in the continued presence of compound, over the next 7 days. RFU = relative fluorescence units. The data shown are the mean ± SEM from two independent biological replicates, each consisting of 3 technical replicates at all time points. **(B)** The data from day 5 (D5) of the growth assay shown in panel (A) were used to calculate the IC_{50} of KNX-002 for parasite growth (16.2 μM, 95% C.I. = 13.0 to 20.5). See Figure 5A for a repeat of these growth assays and IC_{50} calculations. **(C)** Non-confluent HepG2 and HFF cells were cultured in the presence of 0 (DMSO vehicle only), 40, or 80μM KNX-002 for 72 hours. Cell viability/growth was measured using Promega CellTiter-Glo® (top panel) and toxicity was measured using Promega CellTox™ green (bottom panel). 0.1% w/v NaN_3 served as a positive control for cytotoxicity / growth inhibition. Results are plotted relative to the DMSO controls. Bars show the mean of three independent experiments ± SEM. KNX-002 shows no evidence of cytotoxicity or growth inhibition in either cell type at either 40 or 80μM.

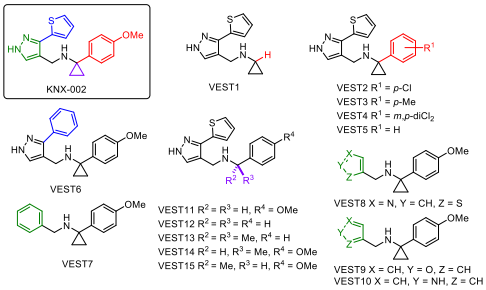

Compound	MyoA ATPase	Parasite growth IC_{50} (95% C.I.)	Toxicity			
			HepG2 cells		HFF cells	
			80 µM	40 µM	80 µM	40 µM
DMSO	1.74 ± 0.10					
KNX-002	0.35 ± 0.06	19.7 (17.8-21.7)	none	none	none	none
VEST1	1.71 ± 0.15	> 80 µM	none	none	none	none
VEST2	0.24 ± 0.03	15.5 (14.2-16.9)	moderate	none	mild	mild
VEST3	0.66 ± 0.02	25.4 (23.3-27.6)	moderate	none	mild	none
VEST4	0.59 ± 0.06	31.0 (27.5-34.6)	none	none	none	mild
VEST5	1.21 ± 0.12	9.9 (9.0-10.8)	none	none	none	none
VEST6	0.71 ± 0.04	24.9 (22.5-27.4)	none	none	none	none
VEST7	1.62 ± 0.16	> 80 µM	none	none	none	none
VEST8	1.69 ± 0.15	> 80 µM	none	none	none	none
VEST9	1.72 ± 0.13	> 80 µM	none	none	none	none
VEST10	1.72 ± 0.10	21.7 (18.7-25.1)	none	none	none	none
VEST11	1.74 ± 0.22	> 80 µM	none	none	none	none
VEST12	1.69 ± 0.14	> 80 µM	none	none	mild	none
VEST13	1.70 ± 0.12	27.1 (20.1-37.1)	none	none	mild	none
VEST14	1.64 ± 0.16	44.3 (41.9-47.1)	none	none	mild	none
VEST15	1.46 ± 0.13	39.7 (34.8-44.8)	none	none	mild	none

Figure 3: Preliminary structure-activity relationship (SAR) analysis. The structures of KNX-002 and 15 analogs (VEST1-15) are shown at the top. The table summarizes the activity of each of the compounds in assays measuring recombinant TgMyoA ATPase activity, parasite growth and mammalian cell toxicity; the data on which the table is based are shown in Suppl. Figures 3-5. ATPase assay data correspond to relative luminescence units x 10^{-6} (mean from 3 independent replicates +/-SEM) in the presence of 20 µM compound (Suppl. Figure 3). Green = less than 20% inhibition, yellow = 20-40% inhibition; orange = 45-70% inhibition; red = greater than 70% inhibition compared to vehicle (DMSO) controls. Growth assay data correspond to calculated IC_{50} and 95% confidence interval from a 5-6 day growth assay (Suppl. Figure 4). Red = IC_{50} less than 20 µM; orange = IC_{50} of 20-35 µM; yellow = IC_{50} of 35-50 µM; green = no detectable growth inhibition relative to vehicle (DMSO) controls. Toxicity assay entries summarize the results from 72-hour CellTox™ Green toxicity and CellTiter-Glo® viability assays on both human foreskin fibroblasts and HepG2 cells. Thresholds for mild and moderate toxicity and loss of viability compared to vehicle (DMSO) controls are indicated by the colored bars on the right hand side of Suppl. Figure 5.

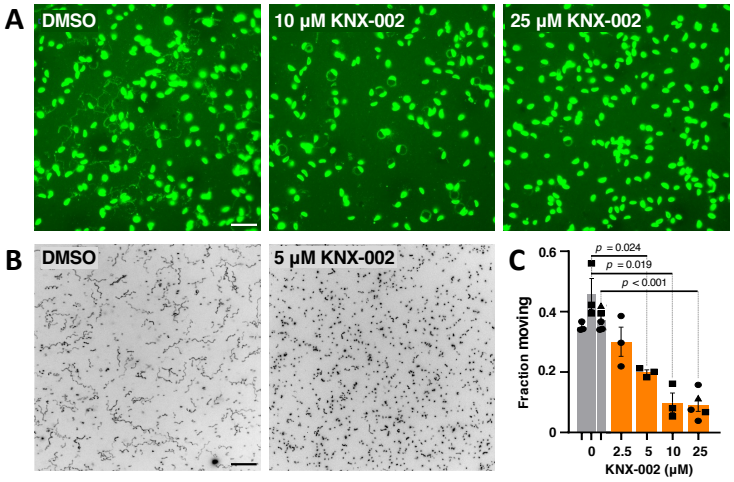

<u>Figure 4</u>: KNX-002 inhibits the motility of *T. gondii* tachyzoites (A) Representative images from a 2D trail assay of parasites treated with DMSO (vehicle) only, 10 μM KNX-002, or 25 μM KNX-002. The parasites and trails were visualized by indirect immunofluorescence using an antibody against TgSAG1 after 15 min of gliding on the coverslip. Scale bar = 20 μm. **(B)** Representative maximum intensity projections showing parasite trajectories during 60 sec of motility in Matrigel in the absence (DMSO) or presence of 5 μM KNX-002. Scale bar = 40 μm. The grayscale images were inverted to provide clearer visualization of the trajectories. **(C)** Fraction of the parasite population moving during a 60 sec assay in the presence of the indicated concentrations of KNX-002 (IC_{50} = 5.3 μM, 95% C.I. = 3.1 – 7.8 μM). Each data point represents a single biological replicate consisting of three technical replicates. Sets of data captured on the same days, indicated by the similar symbol shapes, were compared by Student's one-tailed paired t-tests.

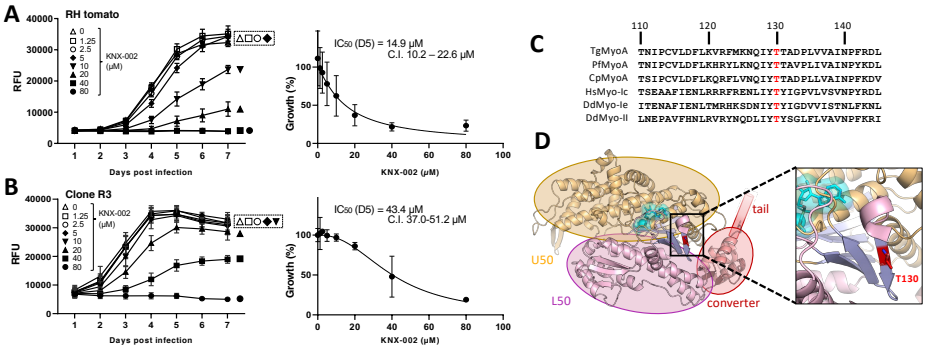

<u>Figure 5</u>: Identification of a mutant parasite showing reduced sensitivity to KNX-002 in growth assays. (A, B) Left panels: tdTomato-expressing wild-type parasites (A) or clone 3R (B), which was generated by mutagenesis and selection in KNX-002, were preincubated with various concentrations of KNX-002 for 5 minutes and then added to HFF cells on a 384-well plate. Fluorescence was measured daily over the next 7 days to quantify parasite growth in the continuing presence of compound. RFU = relative fluorescence units. The data shown are from three independent biological replicates, each consisting of 2-3 technical replicates at all time points. Right panels: the data from day 5 (D5) of the growth assays were used to calculate the IC_{50} and 95% confidence intervals (C.I.) of KNX-002 for parasite growth. Vertical bars indicate SEM (left panels) or 95% C.I. (right panels). **(C)** Multiple sequence alignment showing the high degree of conservation of T130 in apicomplexan MyoAs (Tg = *T. gondii*, Pf = *Plasmodium falciparum*, Cp = *Cryptosporidium parvum*) and MyoIc, Ie and II from *Homo sapiens* (Hs) and *Dictyostelium discoideum* (Dd). **(D)** Structure of the TgMyoA (PDB ID [6DUE]) motor domain, showing the position of T130 (red) relative to the converter, U50 and L50 subdomains.

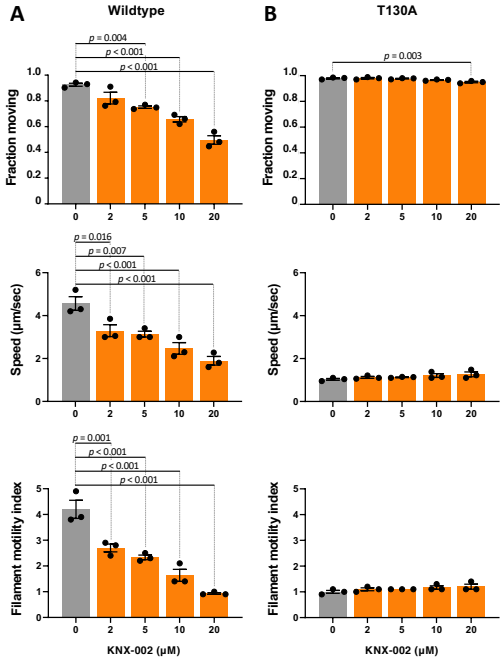

<u>Figure 6</u>: KNX-002 inhibits *in vitro* motility driven by wildtype but not T130A TgMyoA. *In vitro* motility assays, showing the fraction of actin filaments moving, their sliding speed, and the corresponding filament motility Index (fraction moving x mean speed) of TgMyoA treated with various concentrations of KNX-002, as indicated (0 = DMSO vehicle only). **(A)** Wildtype TgMyoA, **(B)** T130A TgMyoA. Bars show the mean of three independent experiments ± SEM. For each motility parameter, compound treatments were compared to DMSO by one-way ANOVA with Dunnett's test for multiple comparisons. Only the statistically significant differences ($p < 0.05$) are indicated.

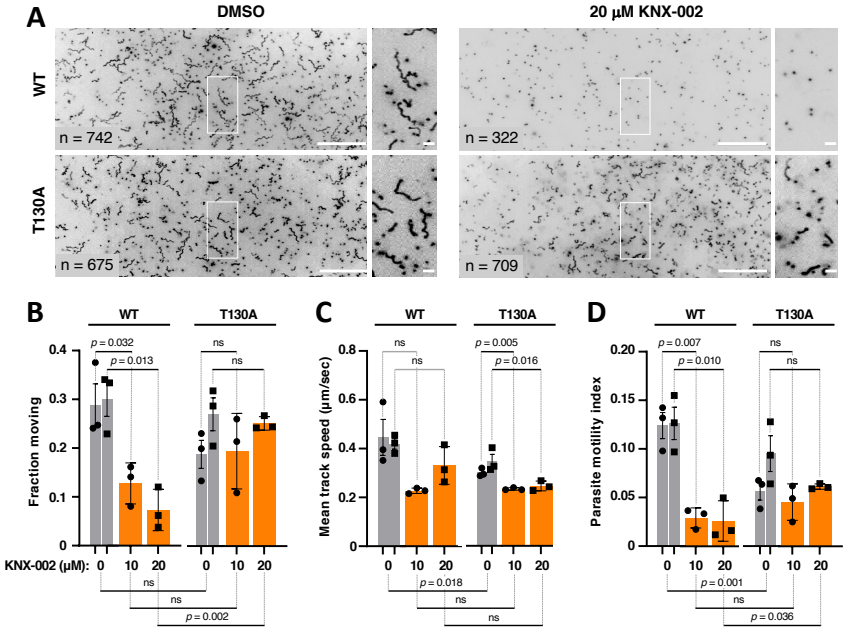

<u>Figure 7</u>: The TgMyoA T130A mutation reduces parasite sensitivity to KNX-002 in 3D motility assays. (A) Large panels: representative maximum intensity projections showing the trajectories of wildtype (WT) and T130A mutant parasites during 80 sec of motility in Matrigel, in the presence of DMSO (vehicle control) or 20 μM KNX-002. The grayscale images were inverted to provide clearer visualization of the trajectories; scale bar = 100 μm. The boxed area in each large panel is magnified and shown on the right; scale bar = 10 μm. **(B)** Percent of wild-type (WT) and T130A mutant parasites moving in the presence of DMSO (vehicle), 10 μM KNX-002, or 20 μM KNX-002. **(C)** The mean speeds of the parasites analyzed in panel B. **(D)** The corresponding parasite motility index (fraction of parasites moving x mean speed). Each data point in panels B-D represents a single biological replicate composed of three technical replicates. Three of the biological replicates were collected on the same three days (circles), and three of the biological replicates were collected on a different three days (squares). Bars show the mean of the biological replicates ± SEM. Sets of biological replicates using the same parasite line and collected on the same days were compared by Student's one-tailed paired t-tests (significance indicated above the graphs). Sets of biological replicates comparing different parasite lines were analyzed by Student's two-tailed unpaired t-tests (significance indicated below the graphs). ns = not significant *(p* > 0.05).

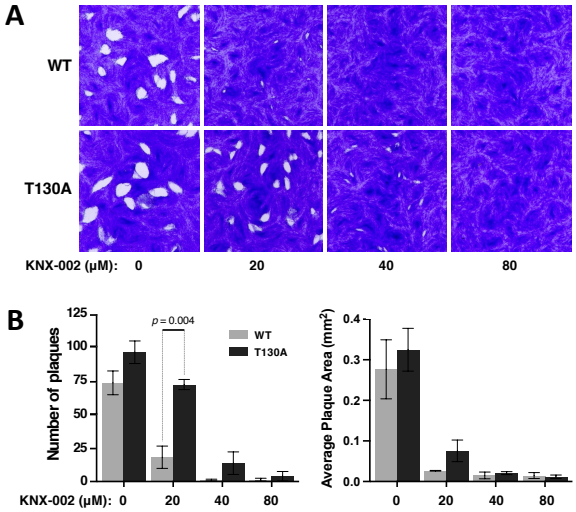

<u>Figure 8</u>: The TgMyoA T130A mutation reduces parasite sensitivity to KNX-002 in growth assays. **(A)** Representative images of plaque assays using wild-type (WT; top row) and T130A mutant (bottom row) parasites in the presence of 0 (DMSO vehicle only), 20, 40, and 80 μM KNX-002, 7 days after inoculating confluent HFF monolayers with 200 parasites/well. An 11.3 X 11.3 mm area from the middle of the well is shown; scale bar = 1 mm. **(B)** Total number of plaques per well and average plaque area of HFF monolayers inoculated with 200 parasites/well (WT or T130A) and grown for 7 days in the presence of 0 (DMSO), 20, 40, or 80 μM KNX-002. Bars show the mean of three biological replicates ± SEM. Treatments were compared by Student's two-tailed unpaired t-test; only the statistically significant differences ($p < 0.05$) are indicated.

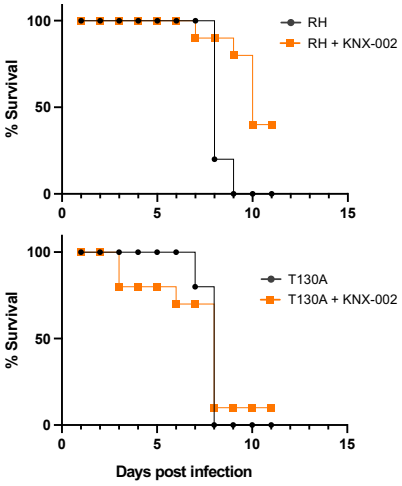

<u>Figure 9</u>: KNX-002 slows disease progression in mice infected with wild-type but not T130A mutant parasites. Four groups of mice were injected intraperitoneally on day 0 with either KNX-002 (20mg/kg) or the equivalent volume of DMSO (vehicle). Thirty minutes later, the mice were infected with 500 wild-type parasites (RH; top panel) or 500 parasites expressing T130A mutant myosin (bottom panel). On day 2, the mice were treated again either with compound or DMSO. Differences between the survival curves were analyzed using a log-rank Mantel-Cox test (p = 0.004 for RH *vs* RH + KNX-002 [top panel]; p = 0.922 for T130A *vs* T130A + KNX-002 [bottom panel]); and p=0.008 for RH + KNX-002 *vs* T130A + KNX-002 (orange curves).

Table 1: Primers and oligonucleotides used in this study

Primer/oligonucleotide	Description	Sequence
P1	Cas9 Vector Protospacer_F	GCTGAGAATTCGAATCAAATCTACACGACTGGTTTTAGAGCTAGAAATAGC
P2	Cas9 Vector Protospacer_R	GCTGAGAATTCAACTTGACATCCCCATTTAC
P3	ds repair: MyoABgIT130APAM_F	GCGTCCTCGACTTCCTCAAGGTGCGCTTCATGAAGAATCAGATCTACGCGACTGCAGACCCGCTCGTCGTCGCCATCAATCCCTTCCGCGA
P4	ds repair: MyoABgIT130APAM_R	TCGCGGAAGGGATTGATGGCGACGACGAGCGGGTCTGCAGTCGCGTAGATCTGATTCTTCATGAAGCGCACCTTGAGGAAGTCGAGGACGC
P5	MyoA Sequencing: LT_BamHI	GCGGGGATCCATGGCGAGCAAGACCACGTCTG
P6	MyoA Sequencing: RK 41	CTGCGTCCAGATCGATCC
P7	MyoA Sequencing: R300	CTTGAGGAAGTCGAGGACG
P8	MyoA Sequencing: F600	GAGGCGACGAAGCAGATTAT
P9	MyoA Sequencing: R1000	TCCACTCACGATGCTCCACA
P10	MyoA Sequencing: F1200	ATCCGCGGCCGGTGGAAGC
P11	MyoA Sequencing: R1600	CGAGAGGAACTTTTCGTCG
P12	MyoA Sequencing: F1900	GTCATGGAGAAGGGGAAGAT
P13	MyoA Sequencing: LT_EcoRI	GGGGGAATTCCTACTACTAGAACGCCGGCTGAACAG
P14	5′ MLC Primer	AACGAAATTGTCCAGCCTT
P15	3′ MLC Primer	AAACAGCTGTCCACACACAAA
P16	MLC1 seqF (int)	CTTCGTGATCTCTCTCCG
P17	ELC1 seqF(int)1	GTCCGCAGCAGAGAGAAACCG
P18	ELC1 seqR(int)1	GTCGCGGCCAGAGATCTCAC
P19	ELCF2	GTGAGATCTCTGGCCGCGAC
P20	ELCR2	CTTCCAGCAGCTCTCGCC
P21	TgMyoA SDM T130A F	AGAATCAAATCTACGCGACTGCGGACCCGC
P22	TgMyoA SDM T130A R	GCGGGTCCGCAGTCGCGTAGATTTGATTCT